Synchronization in Complex Oscillator Networks and Smart Grids

Florian Dörfler [*] [†], **Michael Chertkov** [†], **and Francesco Bullo** [*]

[*]Center for Control, Dynamical Systems and Computation, University of California at Santa Barbara, Santa Barbara, CA 93106, USA, and [†]Center for Nonlinear Studies and Theory Division, Los Alamos National Laboratory, NM 87545, USA

The emergence of synchronization in a network of coupled oscillators is a fascinating topic in various scientific disciplines. A widely-adopted model of a coupled oscillator network is characterized by a population of heterogeneous phase oscillators, a graph describing the interaction among them, and diffusive and sinusoidal coupling. It is known that a strongly coupled and sufficiently homogeneous network synchronizes, but the exact threshold from incoherence to synchrony is unknown. Here we present a novel, concise, and closed-form condition for synchronization of the fully nonlinear, non-equilibrium, and dynamic network. Our synchronization condition can be stated elegantly in terms of the network topology and parameters, or equivalently in terms of an intuitive, linear, and static auxiliary system. Our results significantly improve upon the existing conditions advocated thus far, they are provably exact for various interesting network topologies and parameters, they are statistically correct for almost all networks, and they can be applied equally to synchronization phenomena arising in physics and biology as well as in engineered oscillator networks such as electric power networks. We illustrate the validity, the accuracy, and the practical applicability of our results in complex networks scenarios and in smart grid applications.

synchronization | complex networks | power grids | nonlinear dynamics

The scientific interest in the synchronization of coupled oscillators can be traced back to Christiaan Huygens' seminal work on "an odd kind sympathy" between coupled pendulum clocks [1], and it continues to fascinate the scientific community to date [2, 3]. A mechanical analog of a coupled oscillator network is shown in Figure 1 and consists of a group of particles constrained to rotate around a circle and assumed to move without colliding. Each particle is characterized by a phase angle θ_i and has a preferred natural rotation frequency ω_i. Pairs of interacting particles i and j are coupled through an elastic spring with stiffness a_{ij}. Intuitively, a weakly coupled oscillator network with strongly heterogeneous natural frequencies ω_i does not display any coherent behavior, whereas a strongly coupled network with sufficiently homogeneous natural frequencies is amenable to synchronization. These two qualitatively distinct regimes are illustrated in Figure 1.

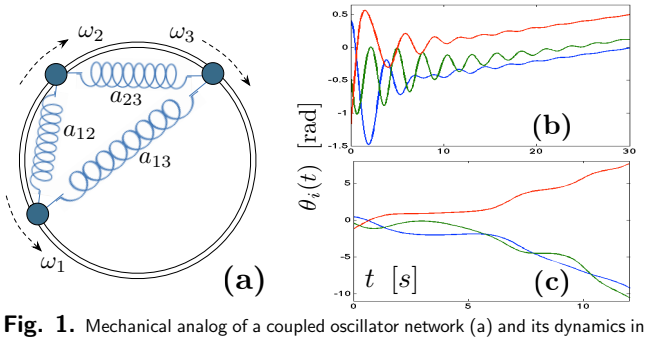

Fig. 1. Mechanical analog of a coupled oscillator network (a) and its dynamics in a strongly coupled (b) and weakly coupled (c) network. With exception of the coupling weights a_{ij}, all parameters in the simulation (b) and (c) are identical.

Formally, the interaction among n such phase oscillators is modeled by a connected graph $G(\mathcal{V}, \mathcal{E}, A)$ with nodes $\mathcal{V} = \{1, \dots, n\}$, edges $\mathcal{E} \subset \mathcal{V} \times \mathcal{V}$, and positive weights $a_{ij} > 0$ for each undirected edge $\{i, j\} \in \mathcal{E}$. For pairs of non-interacting oscillators i and j, the coupling weight a_{ij} is zero. We assume that the node set is partitioned as $\mathcal{V} = \mathcal{V}_1 \cup \mathcal{V}_2$, and we consider the following general coupled oscillator model:

$$\begin{aligned} M_i\ddot{\theta}_i + D_i\dot{\theta}_i &= \omega_i - \sum_{j=1}^{n} a_{ij} \sin(\theta_i - \theta_j)\,, \qquad i \in \mathcal{V}_1\,, \\ D_i\dot{\theta}_i &= \omega_i - \sum_{j=1}^{n} a_{ij} \sin(\theta_i - \theta_j)\,, \qquad i \in \mathcal{V}_2\,. \end{aligned} \tag{1}$$

The coupled oscillator model (1) consists of the second-order oscillators $\mathcal{V}_1$ with Newtonian dynamics, inertia coefficients M_i, and viscous damping D_i. The remaining oscillators $\mathcal{V}_2$ feature first-order dynamics with time constants D_i. A perfect electrical analog of the coupled oscillator model (1) is given by the classic structure-preserving power network model [4], our enabling application of interest. Here, the first and second-order dynamics correspond to loads and generators, respectively, and the right-hand sides depict the power injections ω_i and the power flows $a_{ij} \sin(\theta_i - \theta_j)$ along transmission lines.

The rich dynamic behavior of the coupled oscillator model (1) arises from a competition between each oscillator's tendency to align with its natural frequency ω_i and the synchronization-enforcing coupling $a_{ij} \sin(\theta_i - \theta_j)$ with its neighbors. If all natural frequencies ω_i are identical, then the coupled oscillator dynamics (1) collapse to a trivial phase-synchronized equilibrium, where all angles θ_i are aligned. The dissimilar natural frequencies ω_i, on the other hand, drive the oscillator network away from this all-aligned equilibrium. Moreover, even if the coupled oscillator model (1) synchronizes, the motion of its center of mass still carries the flux of angular rotation, respectively, the flux of electric power from generators to loads in a power grid. In spite of all these complications, the main result of this article is that, for a broad range of network topologies and parameters, an elegant and easy to verify criterion characterizes synchronization of the nonlinear and non-equilibrium dynamic oscillator model (1).

Review of Synchronization in Oscillator Networks

The coupled oscillator model (1) unifies various models in the literature including dynamic models of electric power networks. The supplementary information (SI) discusses modeling of electric power networks in detail. For $\mathcal{V}_2 = \emptyset$, the coupled oscillator model (1) appears in synchronization phenomena in animal flocking behavior [5], populations of flashing fireflies [6], crowd synchrony on London's Millennium bridge [7], as well as Huygen's pendulum clocks [8]. For $\mathcal{V}_1 = \emptyset$, the coupled oscillator model (1) reduces to the celebrated Kuramoto model [9], which appears in coupled Josephson junctions [10], particle coordination [11], spin glass models [12, 13], neuroscience [14], deep brain stimulation [15], chemical oscillations [16], biological locomotion [17], rhythmic applause [18], and countless other synchronization phenomena [19, 20, 21]. Finally, coupled oscillator models of the form (1) are canonical

models of coupled limit cycle oscillators [22] and serve as prototypical examples in complex networks studies [23, 24, 25].

The coupled oscillator dynamics [**1**] feature the synchronizing effect of the coupling described by the graph $G(\mathcal{V}, \mathcal{E}, A)$ and the de-synchronizing effect of the dissimilar natural frequencies ω_i. The complex network community asks questions of the form "what are the conditions on the coupling and the dissimilarity such that a synchronizing behavior emerges?" Similar questions appear also in all the aforementioned applications, for instance, in large-scale electric power systems. Since synchronization is pervasive in the operation of an interconnected power grid, a central question is "under which conditions on the network parameters and topology, the current load profile and power generation, does there exist a synchronous operating point [26, 27], when is it optimal [28], when is it stable [29, 30], and how robust is it [31, 32, 33, 34]?" A local loss of synchrony can trigger cascading failures and possibly result in wide-spread blackouts. In the face of the complexity of future smart grids and the integration challenges posed by renewable energy sources, a deeper understanding of synchronization is increasingly important.

Despite the vast scientific interest, the search for sharp, concise, and closed-form synchronization conditions for coupled oscillator models of the form [**1**] has been so far in vain. Loosely speaking, synchronization occurs when the coupling dominates the dissimilarity. Various conditions have been proposed to quantify this trade-off [21, 34, 30, 25, 35, 23, 24, 33, 36]. The coupling is typically quantified by the nodal degree or the algebraic connectivity of the graph G, and the dissimilarity is quantified by the magnitude or the spread of the natural frequencies ω_i. Sometimes, these conditions can be evaluated only numerically since they depend on the network state [34, 33] or arise from a non-trivial linearization process, such as the Master stability function formalism [23, 24]. To date, exact synchronization conditions are known only for simple coupling topologies [17, 21, 37, 38]. For arbitrary topologies only sufficient conditions are known [34, 30, 25, 35, 33] as well as numerical investigations for random networks [39, 40, 41]. Simulation studies indicate that the known sufficient conditions are very conservative estimates on the threshold from incoherence to synchrony. Literally, every review article on synchronization concludes emphasizing the quest for exact synchronization conditions for arbitrary network topologies and parameters [20, 21, 19, 23, 24]. In this article, we present a concise and sharp synchronization condition which features elegant graph-theoretic and physical interpretations.

Novel Synchronization Condition

For the coupled oscillator model [**1**] and its applications, the following notions of synchronization are appropriate. First, a solution has *synchronized frequencies* if all frequencies $\dot{\theta}_i$ are identical to a common constant value ω_{sync}. If a synchronized solution exists, it is known that the synchronization frequency is $\omega_{\text{sync}} = \sum_{k=1}^{n} \omega_k / \sum_{k=1}^{n} D_k$ and that, by working in a rotating reference frame, one may assume $\omega_{\text{sync}} = 0$. Second, a solution has *cohesive phases* if every pair of connected oscillators has phase distance smaller than some angle $\gamma \in [0, \pi/2[$, that is, $|\theta_i - \theta_j| \leq \gamma$ for every edge $\{i, j\} \in \mathcal{E}$.

Based on a novel analysis approach to the synchronization problem, we propose the following synchronization condition for the coupled oscillator model [**1**]:

> **Sync condition:** The coupled oscillator model [**1**] has a unique and stable solution θ^* with synchronized frequencies and cohesive phases $|\theta_i^* - \theta_j^*| \leq \gamma < \pi/2$ for every pair of connected oscillators $\{i, j\} \in \mathcal{E}$ if
>
> $$\left\| L^{\dagger} \omega \right\|_{\mathcal{E},\infty} \leq \sin(\gamma)\,. \qquad [\mathbf{2}]$$
>
> Here, $L^{\dagger}$ is the pseudo-inverse of the network Laplacian matrix L and $\|x\|_{\mathcal{E},\infty} = \max_{\{i,j\}\in\mathcal{E}} |x_i - x_j|$ is the worst-case dissimilarity for $x = (x_1, \ldots, x_n)$ over the edges $\mathcal{E}$.

We establish the broad applicability of the proposed condition [**17**] to various classes of networks via analytical and statistical methods in the next section. Before that, we provide some equivalent formulations for condition [2] in order to develop deeper intuition and obtain insightful conclusions.

Complex network interpretation: Surprisingly, topological or spectral connectivity measures such as nodal degree or algebraic connectivity are not key to synchronization. In fact, these often advocated [34, 30, 35, 33, 25, 23, 24] connectivity measures turn out to be conservative estimates of the synchronization condition [**17**]. This statement can be seen by introducing the matrix U of orthonormal eigenvectors of the network Laplacian matrix L with corresponding eigenvalues $0 = \lambda_1 < \lambda_2 \leq \cdots \leq \lambda_n$. From this spectral viewpoint, condition [**17**] can be equivalently written as

$$\left\| U \operatorname{diag}\big(0, 1/\lambda_2, \ldots, 1/\lambda_n\big) \cdot \big(U^T \omega\big) \right\|_{\mathcal{E},\infty} \leq \sin(\gamma)\,. \qquad [\mathbf{3}]$$

In words, the natural frequencies ω are projected on the network modes U, weighted by the inverse Laplacian eigenvalues, and $\|\cdot\|_{\mathcal{E},\infty}$ evaluates the worst-case dissimilarity of this weighted projection. A sufficient condition for the inequality [**3**] to be true is the algebraic connectivity condition $\lambda_2 \geq \|\omega\|_{\mathcal{E},\infty} \cdot \sin(\gamma)$. Likewise, a necessary condition for inequality [**3**] is $2 \cdot \deg(G) \geq \lambda_n \geq \|\omega\|_{\mathcal{E},\infty} \cdot \sin(\gamma)$, where $\deg(G)$ is the maximum nodal degree in the graph $G(\mathcal{V}, \mathcal{E}, A)$. Clearly, when compared to [**3**], this sufficient condition and this necessary condition feature only one of $n-1$ non-zero Laplacian eigenvalues and are overly conservative.

Kuramoto oscillator perspective: Notice, that in the limit $\gamma \to \pi/2$, condition [**17**] suggests that there exists a stable synchronized solution if

$$\left\| L^{\dagger} \omega \right\|_{\mathcal{E},\infty} < 1\,. \qquad [\mathbf{4}]$$

For classic Kuramoto oscillators coupled in a complete graph with uniform weights $a_{ij} = K/n$, the synchronization condition [**16**] reduces to the condition $K > \max_{i,j\in\{1,\ldots,n\}} |\omega_i - \omega_j|$, known for the classic Kuramoto model [21].

Power network perspective: In power systems engineering, the equilibrium equations of the coupled oscillator model [**1**], given by $\omega_i = \sum_{j=1}^{n} a_{ij} \sin(\theta_i - \theta_j)$, are referred to as the AC power flow equations, and they are often approximated by their linearization [31, 32, 33, 34] $\omega_i = \sum_{j=1}^{n} a_{ij}(\theta_i - \theta_j)$, known as the DC power flow equations. In vector notation the DC power flow equations read as $\omega = L\theta$, and their solution satisfies $\max_{\{i,j\}\in\mathcal{E}} |\theta_i - \theta_j| = \|L^{\dagger}\omega\|_{\mathcal{E},\infty}$. According to condition [**17**], the worst phase distance $\|L^{\dagger}\omega\|_{\mathcal{E},\infty}$ obtained by the DC power flow equations needs to be less or equal than $\sin(\gamma)$, such that the solution to the AC power flow equations satisfies $\max_{\{i,j\}\in\mathcal{E}} |\theta_i - \theta_j| \leq \gamma$. Hence, our condition extends the common DC power flow approximation from infinitesimally small angles $\gamma \ll 1$ to large angles $\gamma \in [0, \pi/2[$.

Auxiliary linear perspective: As detailed in the previous paragraph, the key term $L^{\dagger}\omega$ in condition [**17**] equals the phase differences obtained by the linear Laplacian equation $\omega = L\theta$. This *linear* interpretation is not only insightful but also practical since condition [**17**] can be quickly evaluated by numerically solving the linear system $\omega = L\theta$. This linear system is possibly of high dimension, but it inherits the sparsity of the graph $G(\mathcal{V}, \mathcal{E}, A)$. Thus, condition [**17**] can be verified efficiently even for large-scale sparse networks. Despite

this linear interpretation, we emphasize that our derivation of condition [17] is not based on any linearization arguments.

Energy landscape perspective: Condition [17] can also be understood in terms of an appealing energy landscape interpretation. The coupled oscillator model [1] is a system of particles that aim to minimize the energy function

$$E(\theta) = \sum\nolimits_{\{i,j\}\in\mathcal{E}} a_{ij}\big(1-\cos(\theta_i-\theta_j)\big) - \sum\nolimits_{i=1}^{n} \omega_i\cdot\theta_i\,,$$

where the first term is a pair-wise nonlinear attraction among the particles, and the second term represents the external force driving the particles away from the "all-aligned" state. Since the energy function $E(\theta)$ is difficult to study, it is natural to look for a minimum of its second-order approximation $E_0(\theta) = \sum_{\{i,j\}\in\mathcal{E}} a_{ij}(\theta_i-\theta_j)^2/2 - \sum_{i=1}^{n}\omega_i\cdot\theta_i$, where the first term corresponds to a Hookean potential. Condition [17] is then restated as follows: $E(\theta)$ features a phase cohesive minimum with interacting particles no further than γ apart if $E_0(\theta)$ features a minimum with interacting particles no further from each other than $\sin(\gamma)$, as illustrated in Figure 2.

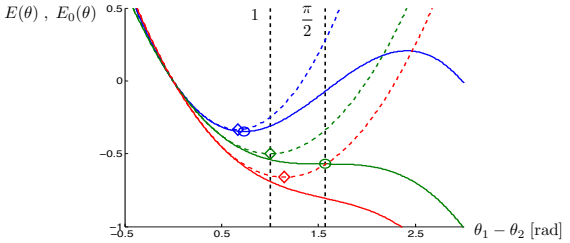

Fig. 2. The energy function $E(\theta)$ and its quadratic approximation $E_0(\theta)$ for a two-particle system are shown as solid and dashed curves, respectively, for the stable (blue), marginal (green) and unstable (red) cases. The circles and diamonds represent stable critical points of $E(\theta)$ and $E_0(\theta)$.

Analytical and Statistical Results

Our analysis approach to the synchronization problem is based on algebraic graph theory. We propose an equivalent reformulation of the synchronization problem, which reveals the crucial role of cycles and cut-sets in the graph and ultimately leads to the synchronization condition [17]. In particular, we analytically establish the synchronization condition [17] for the following six interesting cases:

> **Analytical result:** The synchronization condition [17] is necessary and sufficient for *(i)* the sparsest (acyclic) and *(ii)* the densest (complete and uniformly weighted) network topologies $G(\mathcal{V},\mathcal{E},A)$, *(iii)* the best (phase synchronizing) and *(iv)* the worst (cut-set inducing) natural frequencies, *(v)* for cyclic topologies of length strictly less than five, *(vi)* for arbitrary cycles with symmetric parameters, *(vii)* as well as combinations of networks each satisfying one of the conditions *(i)*-*(vi)*, which are connected to another and share no common cycles.

A detailed and rigorous mathematical derivation and statement of the above analytical result can be found in the SI.

In many applications, the natural frequencies ω_i and coupling weights a_{ij} are known only with a certain degree of accuracy, or they may be variable within certain ranges. For instance, in power networks these variations arise from uncertain demand or unmodeled voltage dynamics. In order to address these uncertainties, condition [17] can be extended to a robust synchronization condition for variable parameters $\underline{\omega_i} \le \omega_i \le \overline{\omega_i}$ and $0 < \underline{a_{ij}} \le a_{ij} \le \overline{a_{ij}}$. In this case, it is necessary and sufficient to verify condition [17] at the vertices of the parameter space $\omega_i \in \{\underline{\omega_i}\,,\,\overline{\omega_i}\}$ and $a_{ij} \in \{\underline{a_{ij}}\,,\,\overline{a_{ij}}\}$ to guarantee condition [17] for all possible parameter variations. The detailed results are reported in the SI.

After having analytically established condition [17] for a variety of particular network topologies and parameters, we establish its correctness and predictive power for a broad range of networks. Extensive simulation studies lead to the conclusion that the proposed synchronization condition [17] is statistically correct. In order to verify this hypothesis, we conducted Monte Carlo simulation studies over a wide range of natural frequencies ω_i, network sizes n, coupling weights a_{ij}, and different random graph models of varying degrees of sparsity and randomness. We select a set of *nominal network* models with topologies constructed from Erdös-Rényi graphs, random geometric graphs, and Watts-Strogatz small world networks, and the natural frequencies and coupling weights are sampled from uniform distributions. In total, we constructed $1.2\cdot10^6$ samples of such nominal networks, each with a connected graph $G(\mathcal{V},\mathcal{E},A)$ and natural frequencies ω satisfying $\|L^\dagger\omega\|_{\mathcal{E},\infty} \le \sin(\gamma)$ for some $\gamma < \pi/2$. The detailed construction and the precise results can be found in the SI and allow us to establish the following probabilistic result with a confidence level of at least 99% and accuracy of at least 99%:

> **Statistical result for nominal networks:** With 99.97 % probability, for a nominal network, condition [17] guarantees the existence of an unique and stable solution θ^* with synchronized frequencies and cohesive phases $|\theta_i^*-\theta_j^*| \le \gamma$ for every connected pair $\{i,j\}\in\mathcal{E}$.

From this statistical result, we deduce that the proposed synchronization condition [17] holds true for *almost all* topologies and parameters of the considered nominal network models. Indeed, we also show the existence of possibly-thin sets of network topologies and parameters for which our condition [17] is not sufficiently tight. We refer to the SI for an explicit family of carefully engineered and "degenerate" counterexamples. Overall, our analytical and statistical results validate the correctness of the proposed condition [17].

After having established the statistical correctness of condition [17], we now investigate its predictive power for arbitrary networks. Since we analytically establish that condition [17] is exact for sufficiently small pairwise phase cohesiveness $|\theta_i-\theta_j| \ll 1$, we now investigate the other extreme, $\max_{\{i,j\}\in\mathcal{E}}|\theta_i-\theta_j| = \pi/2$. To test the corresponding condition [16] in a low-dimensional parameter space, we consider a complex network of Kuramoto oscillators

$$\dot\theta_i = \omega_i - K\cdot\sum\nolimits_{j=1}^{n} a_{ij}\sin(\theta_i-\theta_j)\,,\quad i\in\{1,\dots,n\}\,, \qquad [5]$$

where all coupling weights a_{ij} are either zero or one, and the coupling gain $K>0$ serves as control parameter. If L is the corresponding unweighted Laplacian matrix, then condition [16] reads as $K > K_{\text{critical}} \triangleq \|L^\dagger\omega\|_{\mathcal{E},\infty}$. Of course, the condition $K > K_{\text{critical}}$ is only sufficient and the critical coupling may be smaller than K_{critical}. In order to test the accuracy of the condition $K > K_{\text{critical}}$, we numerically found the smallest value of K leading to synchrony with phase cohesiveness $\pi/2$.

Figure 3 reports our findings for various network sizes, connected random graph models, and sample distributions of the natural frequencies. We refer to the SI for the detailed simulation setup. First, notice from Subfigures (a),(b),(d), and (e) that condition [16] is extremely accurate for a sparse graph, that is, for small p and n, as expected from our analytical results. Second, for a dense graph with $p\approx1$, Subfigures (a),(b),(d), and (e) confirm the results known for classic

Kuramoto oscillators [21]: for a bipolar distribution condition **[16]** is exact, and for a uniform distribution a small critical coupling is obtained. Third, Subfigures (c) and (d) show that condition **[16]** is scale-free for a Watts-Strogatz small world network, that is, it has almost constant accuracy for various values of n and p. Fourth and finally, observe that condition **[16]** is always within a constant factor of the exact critical coupling, whereas other proposed conditions [34, 30, 25, 35, 33, 23, 24] on the nodal degree or on the algebraic connectivity scale poorly with respect to network size n.

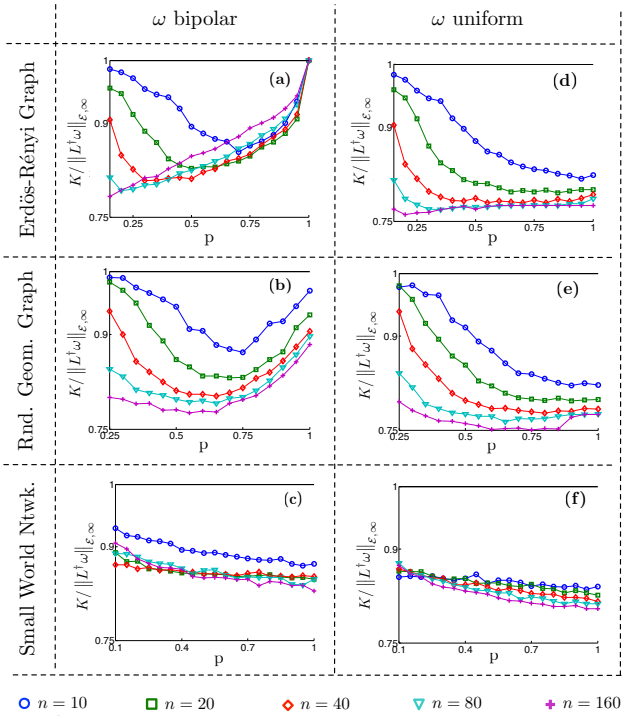

Fig. 3. Numerical evaluation of the exact critical coupling K in a complex Kuramoto oscillator network. The subfigures show K normalized by $\|L^\dagger\omega\|_{\mathcal{E},\infty}$ for an Erdös-Rényi graph with probability p of connecting two nodes, for a random geometric graph with connectivity radius p, and for a Watts-Strogatz small world network with rewiring probability p. Each data point is the mean over 100 samples of the respective random graph model, for values of ω_i sampled from a bipolar or a uniform distribution supported on $[-1, 1]$, and for the network sizes $n \in \{10, 20, 40, 80, 160\}$.

Applications in Power Networks

We envision that condition **[17]** can be applied to quickly assess synchronization and robustness in power networks under volatile operating conditions. Since real-world power networks are carefully engineered systems with particular network topologies and parameters, we do not extrapolate the statistical results from the previous section to power grids. Rather, we consider ten widely-established IEEE power network test cases provided by [42, 43].

Under nominal operating conditions, the power generation is optimized to meet the forecast demand, while obeying the AC power flow laws and respecting the thermal limits of each transmission line. Thermal limits constraints are precisely equivalent to phase cohesiveness requirements. In order to test the synchronization condition **[17]** in a volatile smart grid scenario, we make the following changes to the nominal network: 1) We assume fluctuating demand and randomize 50% of all loads to deviate from the forecasted loads. 2) We assume that the grid is penetrated by renewables with severely fluctuating power outputs, for example, wind or solar farms, and we randomize 33% of all generating units to deviate from the nominally scheduled generation. 3) Following the paradigm of *smart operation of smart grids* [44], the fluctuations can be mitigated by fast-ramping generation, such as fast-response energy storage including batteries and flywheels, and controllable loads, such as large-scale server farms or fleets of plug-in hybrid electrical vehicles. Here, we assume that the grid is equipped with 10% fast-ramping generation and 10% controllable loads, and the power imbalance (caused by fluctuating demand and generation) is uniformly dispatched among these adjustable power sources. For each of the ten IEEE test cases, we construct 1000 random realizations of the scenario 1), 2), and 3) described above, we numerically check for the existence of a synchronous solution, and we compare the numerical solution with the results predicted by our condition **[17]**. Our findings are reported in Table 1, and a detailed description of the simulation setup can be found in the SI.

It can be observed that condition **[17]** predicts the correct phase cohesiveness $|\theta_i - \theta_j|$ along all transmission lines $\{i, j\} \in \mathcal{E}$ with extremely high accuracy even for large-scale networks featuring 2383 nodes. These conclusions can also be extended to power network models with variable parameters which account for uncertainty in demand or unmodeled voltage dynamics. We refer to the SI for further details.

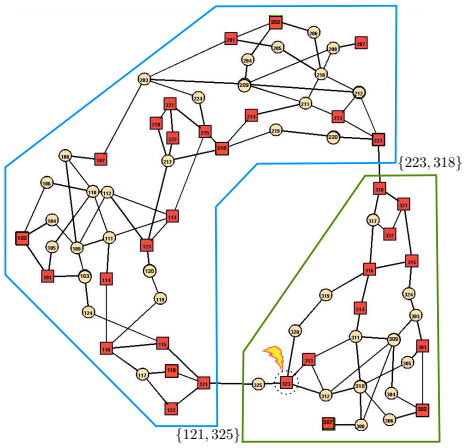

Fig. 4. Illustration of contingencies the RTS 96 power network. Here, square nodes are generators and round nodes are loads, large amounts of power are exported from the Northwestern area to the Southeastern area, and generator 323 is tripped.

As a final test, we validate the synchronization condition **[17]** in a stressed power grid case study. We consider the *IEEE Reliability Test System 96* (RTS 96) [43] illustrated in Figure 4. We assume the following two contingencies have taken place and we characterize the remaining safety margin. First, we assume generator 323 is disconnected, possibly due to maintenance or failure events. Second, we consider the following imbalanced power dispatch situation: the power demand at each load in the Southeastern area deviates from the nominally forecasted demand by a uniform and positive amount, and the resulting power deficiency is compensated by uniformly increasing the generation in the Northwestern area. This imbalance can arise, for example, due to a shortfall in predicted load and renewable energy generation. Correspondingly, power is exported from the Northwestern to the Southeastern area via the transmission lines $\{121, 325\}$ and $\{223, 318\}$. At a nominal operating condition, the RTS 96 power network is sufficiently robust to tolerate each single

one of these two contingencies, but the safety margin is now minimal. When both contingencies are combined, then our synchronization condition [**17**] predicts that the thermal limit of the transmission line $\{121, 325\}$ is reached at an additional loading of 22.20%. Indeed, the dynamic simulation scenario shown in Figure 5 validates the accuracy of this prediction. It can be observed, that synchronization is lost for an additional loading of 22.33%, and the areas separate via the transmission line $\{121, 325\}$. This separation triggers a cascade of events, such as the outage of the transmission line $\{223, 318\}$, and the power network is en route to a blackout. We remark that, if generator 323 is not disconnected and there are no thermal limit constraints, then, by increasing the loading, we observe the classic loss of synchrony through a saddle-node bifurcation. Also this bifurcation can be predicted accurately by our results, see the SI for a detailed description.

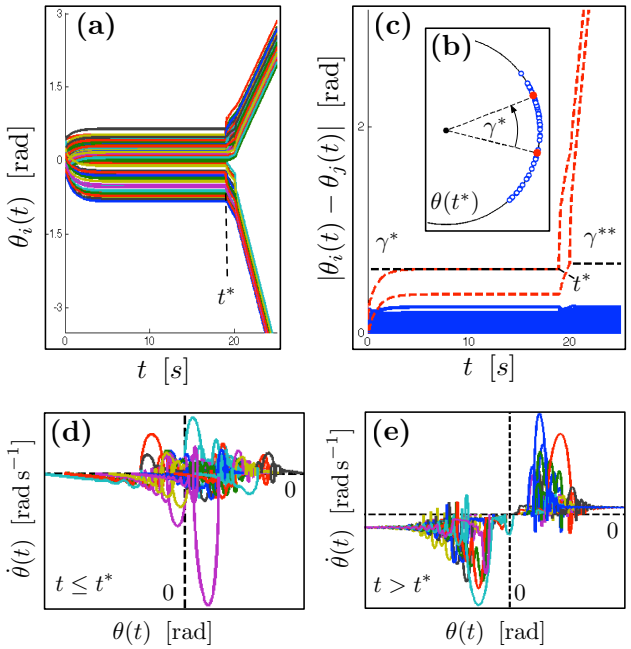

Fig. 5. The RTS 96 dynamics for a continuous load increase from 22.19% to 22.24%. Subfigure (a) shows the angles $\theta(t)$ which loose synchrony at $t^* = 18.94\,\mathrm{s}$, when the thermal limit $\gamma^* = 0.1977\,\mathrm{rad}$ of the transmission line $\{121, 325\}$ is reached. Subfigure (b) shows the angles $\theta(t)$ at $t = t^*$. Subfigure (c) depicts the angular distances and the thermal limits γ^* and γ^{**}, where the lines $\{121, 325\}$ and $\{223, 318\}$ are plotted as dashed curves. Subfigures (d) and (e) show the generator phase space $\big(\theta(t), \dot{\theta}(t)\big)$ before and after t^*, where the loss of a common synchronization frequency can be observed.

In summary, the results in this section confirm the validity, the applicability, and the accuracy of the synchronization condition [**17**] in complex power network scenarios.

Discussion and Conclusions

In this article we studied the synchronization phenomenon for broad class of coupled oscillator models proposed in the scientific literature. We proposed a surprisingly simple condition that accurately predicts synchronization as a function of the parameters and the topology of the underlying network. Our result, with its physical and graph theoretical interpretations, significantly improves upon the existing test in the literature on synchronization. The correctness of our synchronization condition is established analytically for various interesting network topologies and via Monte Carlo simulations for a broad range of generic networks. We validated our theoretical results for complex Kuramoto oscillator networks as well as in smart grid applications.

Our results pose as many questions as they answer. Among the important theoretical problems to be addressed is a characterization of the set of all network topologies and parameters for which our proposed synchronization condition $\|L^\dagger\omega\|_{\mathcal{E},\infty} < 1$ is not sufficiently tight. We conjecture that this set is "thin" in an appropriate parameter space. Our results suggest that an exact condition for synchronization of any arbitrary network is of the form $\|L^\dagger\omega\|_{\mathcal{E},\infty} < c$, and we conjecture that the constant c is always strictly positive, upper-bounded, and close to one. Yet another important question not addressed in the present article concerns the region of attraction of a synchronized solution. We conjecture that the latter depends on the gap in the presented condition.

On the application side, the results contained in this paper need to be extended to more detailed power network models including voltage dynamics, reactive power flows, and higher-order generator dynamics. We envision that our synchronization conditions enable emerging smart grid applications, such as power flow optimization subject to stability constraints, distance to failure metric, and the design of control strategies to avoid cascading failures.

Table 1. Evaluation of condition [17] for ten IEEE test cases under volatile operating conditions.

Randomized test case: (1000 instances):	*Correctness:	†Accuracy: [rad]	‡Cohesive: [rad]
Chow 9 bus system	`always true`	$4.1218 \cdot 10^{-5}$	0.12889
IEEE 14 bus system	`always true`	$2.7995 \cdot 10^{-4}$	0.16622
IEEE RTS 24	`always true`	$1.7089 \cdot 10^{-3}$	0.22309
IEEE 30 bus system	`always true`	$2.6140 \cdot 10^{-4}$	0.16430
New England 39	`always true`	$6.6355 \cdot 10^{-5}$	0.16821
IEEE 57 bus system	`always true`	$2.0630 \cdot 10^{-2}$	0.20295
IEEE RTS 96	`always true`	$2.6076 \cdot 10^{-3}$	0.24593
IEEE 118 bus system	`always true`	$5.9959 \cdot 10^{-4}$	0.23524
IEEE 300 bus system	`always true`	$5.2618 \cdot 10^{-4}$	0.43204
Polish 2383 bus system (winter 99)	`always true`	$4.2183 \cdot 10^{-3}$	0.25144

*Correctness: $\|L^\dagger\omega\|_{\mathcal{E},\infty} \leq \sin(\gamma) \implies \max_{\{i,j\}\in\mathcal{E}} |\theta_i^* - \theta_j^*| \leq \gamma$

†Accuracy: $\big|\max_{\{i,j\}\in\mathcal{E}} |\theta_i^* - \theta_j^*| - \arcsin(\|L^\dagger\omega\|_{\mathcal{E},\infty})\big|$

‡Phase cohesiveness: $\max_{\{i,j\}\in\mathcal{E}} |\theta_i^* - \theta_j^*|$

¶The accuracy and phase cohesiveness results are averaged over 1000 instances of randomized load and generation.

ACKNOWLEDGMENTS. This material is based in part upon work supported by NSF grants IIS-0904501 and CPS-1135819. Research at LANL was carried out under the auspices of the National Nuclear Security Administration of the U.S. Department of Energy at Los Alamos National Laboratory under Contract No. DE C52-06NA25396.

1. Huygens, C. Horologium Oscillatorium (Paris, France, 1673).
2. Strogatz, S. H. SYNC: The Emerging Science of Spontaneous Order (Hyperion, 2003).
3. Winfree, A. T. The Geometry of Biological Time (Springer, 2001), 2 edn.
4. Bergen, A. R. & Hill, D. J. A structure preserving model for power system stability analysis. IEEE Transactions on Power Apparatus and Systems 100, 25–35 (1981).
5. Ha, S. Y., Jeong, E. & Kang, M. J. Emergent behaviour of a generalized Viscek-type flocking model. Nonlinearity 23, 3139–3156 (2010).
6. Ermentrout, G. B. An adaptive model for synchrony in the firefly pteroptyx malaccae. Journal of Mathematical Biology 29, 571–585 (1991).
7. Strogatz, S. H., Abrams, D. M., McRobie, A., Eckhardt, B. & Ott, E. Theoretical mechanics: Crowd synchrony on the Millennium Bridge. Nature 438, 43–44 (2005).
8. Bennett, M., Schatz, M. F., Rockwood, H. & Wiesenfeld, K. Huygens's clocks. Proceedings: Mathematical, Physical and Engineering Sciences 458, 563–579 (2002).
9. Kuramoto, Y. Self-entrainment of a population of coupled non-linear oscillators. In Araki, H. (ed.) Int. Symposium on Mathematical Problems in Theoretical Physics, vol. 39 of Lecture Notes in Physics, 420–422 (Springer, 1975).
10. Wiesenfeld, K., Colet, P. & Strogatz, S. H. Frequency locking in Josephson arrays: Connection with the Kuramoto model. Physical Review E 57, 1563–1569 (1998).
11. Paley, D. A., Leonard, N. E., Sepulchre, R., Grunbaum, D. & Parrish, J. K. Oscillator models and collective motion. IEEE Control Systems Magazine 27, 89–105 (2007).
12. Jongen, G., Anemüller, J., Bollé, D., Coolen, A. C. C. & Perez-Vicente, C. Coupled dynamics of fast spins and slow exchange interactions in the XY spin glass. Journal of Physics A: Mathematical and General 34, 3957–3984 (2001).
13. Daido, H. Quasientrainment and slow relaxation in a population of oscillators with random and frustrated interactions. Physical Review Letters 68, 1073–1076 (1992).
14. Varela, F., Lachaux, J. P., Rodriguez, E. & Martinerie, J. The brainweb: Phase synchronization and large-scale integration. Nature Reviews Neuroscience 2, 229–239 (2001).
15. Tass, P. A. A model of desynchronizing deep brain stimulation with a demand-controlled coordinated reset of neural subpopulations. Biological Cybernetics 89, 81–88 (2003).
16. Kiss, I. Z., Zhai, Y. & Hudson, J. L. Emerging coherence in a population of chemical oscillators. Science 296, 1676 (2002).
17. Kopell, N. & Ermentrout, G. B. Coupled oscillators and the design of central pattern generators. Mathematical Biosciences 90, 87–109 (1988).
18. Néda, Z., Ravasz, E., Vicsek, T., Brechet, Y. & Barabási, A. L. Physics of the rhythmic applause. Physical Review E 61, 6987 (2000).
19. Strogatz, S. H. From Kuramoto to Crawford: Exploring the onset of synchronization in populations of coupled oscillators. Physica D: Nonlinear Phenomena 143, 1–20 (2000).
20. Acebrón, J. A., Bonilla, L. L., Vicente, C. J. P., Ritort, F. & Spigler, R. The Kuramoto model: A simple paradigm for synchronization phenomena. Reviews of Modern Physics 77, 137–185 (2005).
21. Dörfler, F. & Bullo, F. On the critical coupling for Kuramoto oscillators. SIAM Journal on Applied Dynamical Systems 10, 1070–1099 (2011).
22. Hoppensteadt, F. C. & Izhikevich, E. M. Weakly connected neural networks, vol. 126 (Springer, 1997).
23. Arenas, A., Díaz-Guilera, A., Kurths, J., Moreno, Y. & Zhou, C. Synchronization in complex networks. Physics Reports 469, 93–153 (2008).
24. Boccaletti, S., Latora, V., Moreno, Y., Chavez, M. & Hwang, D. U. Complex networks: Structure and dynamics. Physics Reports 424, 175–308 (2006).
25. Dörfler, F. & Bullo, F. Exploring synchronization in complex oscillator networks. In IEEE Conf. on Decision and Control (Maui, HI, USA, 2012). To appear.
26. Lesieutre, B. C., Sauer, P. W. & Pai, M. A. Existence of solutions for the network/load equations in power systems. IEEE Transactions on Circuits and Systems I: Fundamental Theory and Applications 46, 1003–1011 (1999).
27. Dobson, I. Observations on the geometry of saddle node bifurcation and voltage collapse in electrical power systems. IEEE Transactions on Circuits and Systems I: Fundamental Theory and Applications 39, 240–243 (1992).
28. Lavaei, J., Tse, D. & Zhang, B. Geometry of power flows in tree networks. IEEE Power & Energy Society General Meeting (2012).
29. Hill, D. J. & Chen, G. Power systems as dynamic networks. In IEEE Int. Symposium on Circuits and Systems, 722–725 (Kos, Greece, 2006).
30. Dörfler, F. & Bullo, F. Synchronization and transient stability in power networks and non-uniform Kuramoto oscillators. SIAM Journal on Control and Optimization 50, 1616–1642 (2012).
31. Ilić, M. Network theoretic conditions for existence and uniqueness of steady state solutions to electric power circuits. In IEEE International Symposium on Circuits and Systems, 2821–2828 (San Diego, CA, USA, 1992).
32. Araposthatis, A., Sastry, S. & Varaiya, P. Analysis of power-flow equation. International Journal of Electrical Power & Energy Systems 3, 115–126 (1981).
33. Wu, F. & Kumagai, S. Steady-state security regions of power systems. IEEE Transactions on Circuits and Systems 29, 703–711 (1982).
34. Wu, F. F. & Kumagai, S. Limits on Power Injections for Power Flow Equations to Have Secure Solutions (Electronics Research Laboratory, College of Engineering, University of California, 1980).
35. Jadbabaie, A., Motee, N. & Barahona, M. On the stability of the Kuramoto model of coupled nonlinear oscillators. In American Control Conference, 4296–4301 (Boston, MA, USA, 2004).
36. Buzna, L., Lozano, S. & Diaz-Guilera, A. Synchronization in symmetric bipolar population networks. Physical Review E 80, 66120 (2009).
37. Strogatz, S. H. & Mirollo, R. E. Phase-locking and critical phenomena in lattices of coupled nonlinear oscillators with random intrinsic frequencies. Physica D: Nonlinear Phenomena 31, 143–168 (1988).
38. Verwoerd, M. & Mason, O. On computing the critical coupling coefficient for the Kuramoto model on a complete bipartite graph. SIAM Journal on Applied Dynamical Systems 8, 417–453 (2009).
39. Gómez-Gardenes, J., Moreno, Y. & Arenas, A. Paths to synchronization on complex networks. Physical Review Letters 98, 34101 (2007).
40. Nishikawa, T., Motter, A. E., Lai, Y. C. & Hoppensteadt, F. C. Heterogeneity in oscillator networks: Are smaller worlds easier to synchronize? Physical Review Letters 91, 14101 (2003).
41. Moreno, Y. & Pacheco, A. F. Synchronization of Kuramoto oscillators in scale-free networks. Europhysics Letters 68, 603 (2004).
42. Zimmerman, R. D., Murillo-Sánchez, C. E. & Gan, D. MATPOWER: Steady-state operations, planning, and analysis tools for power systems research and education. IEEE Transactions on Power Systems 26, 12–19 (2011).
43. Grigg, C. et al. The IEEE Reliability Test System - 1996. A report prepared by the Reliability Test System Task Force of the Application of Probability Methods Subcommittee. IEEE Transactions on Power Systems 14, 1010–1020 (1999).
44. Varaiya, P. P., Wu, F. F. & Bialek, J. W. Smart operation of smart grid: Risk-limiting dispatch. Proceedings of the IEEE 99, 40–57 (2011).

Supplementary Information

Introduction

This supplementary information is organized as follows.

The section *Mathematical Models and Synchronization Notions* provides a description of the considered coupled oscillator model including a detailed modeling of a mechanical analog and a few power network models. Furthermore, we state our definition of synchronization and compare various synchronization conditions proposed for oscillator networks.

The section *Mathematical Analysis of Synchronization* provides a rigorous mathematical analysis of synchronization, which leads to the novel synchronization conditions proposed in the main article. Throughout our analysis we provide various examples illustrating certain theoretical concepts and results, and we also compare our results to existing results in the synchronization and power networks literature.

The section *Robust Synchronization in Presence of Uncertainty* extends our synchronization condition to the case when the network parameters can vary within prescribed upper and lower bounds. This parameter-varying approach can account for modeling uncertainties or unmodeled dynamics.

The section *Statistical Synchronization Assessment* provides a detailed account of our Monte Carlo simulation studies and the complex Kuramoto network studies. Throughout this section, we also recall the basics of probability estimation by Monte Carlo methods that allow us to establish a statistical synchronization result in a mathematically rigorous way.

Finally, the section *Synchronization Assessment for Power Networks* describes the detailed simulation setup for the randomized IEEE test systems, it provides the simulation data used for the dynamic RTS 96 power network simulations, it illustrates a dynamic bifurcation scenario in the RTS 96 power network, and it describes extensions of the results in the main paper to variable load demands and load voltages.

The remainder of this section introduces some notation and recalls some preliminaries.

Preliminaries and Notation. *Vectors and functions:* Let $\mathbf{1}_n$ and $\mathbf{0}_n$ be the n-dimensional vector of unit and zero entries, and let $\mathbf{1}_n^\perp$ be the orthogonal complement of $\mathbf{1}_n$ in $\mathbb{R}^n$, that is, $\mathbf{1}_n^\perp \triangleq \{x \in \mathbb{R}^n : x \perp \mathbf{1}_n\}$. Let e_i^n be ith canonical basis vector of $\mathbb{R}^n$, that is, the ith entry of e_i^n is 1 and all other entries are zero. Let $\mathbf{1}_{n\times n} = \mathbf{1}_n \cdot \mathbf{1}_n^T$ be the $(n \times n)$-matrix of unit entries. Given an n-tuple $(x_1, \dots, x_n)$, let $x \in \mathbb{R}^n$ be the associated vector. For an ordered index set $\mathcal{I}$ of cardinality $|\mathcal{I}|$ and an one-dimensional array $\{x_i\}_{i\in\mathcal{I}}$, we define $\mathrm{diag}(\{x_i\}_{i\in\mathcal{I}}) \in \mathbb{R}^{|\mathcal{I}|\times|\mathcal{I}|}$ to be the associated diagonal matrix. For $x \in \mathbb{R}^n$, define the vector-valued functions $\mathbf{sin}(x) = (\sin(x_1), \dots, \sin(x_n))$ and $\mathbf{arcsin}(x) = (\arcsin(x_1), \dots, \arcsin(x_n))$, where the arcsin function is defined for the branch $[-\pi/2, \pi/2]$. For a set $\mathcal{X} \subset \mathbb{R}^n$ and a matrix $A \in \mathbb{R}^{m\times n}$, let $A\mathcal{X} = \{y \in \mathbb{R}^m : y = Ax\,,\, x \in \mathcal{X}\}$.

Geometry on n-torus: The set $\mathbb{S}^1$ denotes the *unit circle*, an *angle* is a point $\theta \in \mathbb{S}^1$, and an *arc* is a connected subset of $\mathbb{S}^1$. The *geodesic distance* between two angles $\theta_1, \theta_2 \in \mathbb{S}^1$ is the minimum of the counter-clockwise and the clockwise arc length connecting θ_1 and θ_2. With slight abuse of notation, let $|\theta_1 - \theta_2|$ denote the *geodesic distance* between two angles $\theta_1, \theta_2 \in \mathbb{S}^1$. Finally, the *n-torus* is the product set $\mathbb{T}^n = \mathbb{S}^1 \times \cdots \times \mathbb{S}^1$ is the direct sum of n unit circles.

Algebraic graph theory: Given an undirected, connected, and weighted graph $G(\mathcal{V}, \mathcal{E}, A)$ induced by the symmetric, irreducible, and nonnegative *adjacency matrix* $A \in \mathbb{R}^{n\times n}$, the *Laplacian matrix* $L \in \mathbb{R}^{n\times n}$ is defined by $L = \mathrm{diag}(\{\sum_{j=1}^n a_{ij}\}_{i=1}^n) - A$. If a number $\ell \in \{1, \dots, |\mathcal{E}|\}$ and an arbitrary direction is assigned to each edge $\{i, j\} \in \mathcal{E}$, the (oriented) *incidence matrix* $B \in \mathbb{R}^{n\times|\mathcal{E}|}$ is defined componentwise as $B_{k\ell} = 1$ if node k is the sink node of edge ℓ and as $B_{k\ell} = -1$ if node k is the source node of edge ℓ; all other elements are zero. For $x \in \mathbb{R}^n$, the vector $B^T x$ has components $x_i - x_j$ for any oriented edge from j to i, that is, B^T maps node variables x_i, x_j to incremental edge variables $x_i - x_j$. If $\mathrm{diag}(\{a_{ij}\}_{\{i,j\}\in\mathcal{E}})$ is the diagonal matrix of nonzero edge weights, then $L = B\,\mathrm{diag}(\{a_{ij}\}_{\{i,j\}\in\mathcal{E}})B^T$. For a vector $x \in \mathbb{R}^n$, the incremental norm $\|x\|_{\mathcal{E},\infty} \triangleq \max_{\{i,j\}\in\mathcal{E}} |x_i - x_j|$ used in the main article can be expressed via the incidence matrix B as $\|x\|_{\mathcal{E},\infty} = \|B^T x\|_\infty$. If the graph is connected, then $\mathrm{Ker}\,(B^T) = \mathrm{Ker}\,(L) = \mathrm{span}(\mathbf{1}_n)$, all $n-1$ remaining eigenvalues of L are real and strictly positive, and the second-smallest eigenvalue $\lambda_2(L)$ is called the *algebraic connectivity*. The orthogonal vector spaces $\mathrm{Ker}\,(B)$ and $\mathrm{Ker}\,(B)^\perp = \mathrm{Im}\,(B^T)$ are spanned by vectors associated to cycles and cut-sets in the graph , see for example [1, Section 4] or [2]. In the following, we refer to $\mathrm{Ker}\,(B)$ and $\mathrm{Im}\,(B^T)$ as the *cycle space* and the *cut-set space*, respectively.

Laplacian inverses: Since the Laplacian matrix L is singular, we will frequently use its *Moore-Penrose pseudo inverse* $L^\dagger$. If $U \in \mathbb{R}^{n\times n}$ is an orthonormal matrix of eigenvectors of L, the singular value decomposition of L is $L = U\,\mathrm{diag}(\{0, \lambda_2, \dots, \lambda_n\})U^T$, and its Moore-Penrose pseudo inverse $L^\dagger$ is given by $L^\dagger = U\,\mathrm{diag}(\{0, 1/\lambda_2, \dots, 1/\lambda_n\})U^T$. We will frequently use the identity $L \cdot L^\dagger = L^\dagger \cdot L = I_n - \frac{1}{n}\mathbf{1}_{n\times n}$, which follows directly from the singular value decomposition. We also define the *effective resistance* between nodes i and j by $R_{ij} = L^\dagger_{ii} + L^\dagger_{jj} - 2L^\dagger_{ij}$. We refer to [3] for further information on Laplacian inverses and on the resistance distance.

Mathematical Models and Synchronization Notions

In this section we introduce the mathematical model of coupled phase oscillators considered in this article, we present some synchronization notions, and give a detailed account of the literature on synchronization of coupled phase oscillators.

General Coupled Oscillator Model. Consider a weighted, undirected, and connected graph $G(\mathcal{V}, \mathcal{E}, A)$ with n nodes $\mathcal{V} = \{1, \dots, n\}$, partitioned node set $\mathcal{V} = \mathcal{V}_1 \cup \mathcal{V}_2$ and edge set $\mathcal{E}$ induced by the adjacency matrix $A \in \mathbb{R}^{n\times n}$. We assume that the graph G has no self-loops $\{i, i\}$, that is, $a_{ii} = 0$ for all $i \in \mathcal{V}$. Associated to this graph, consider the following model of $|\mathcal{V}_1| \geq 0$ second-order Newtonian and $|\mathcal{V}_2| \geq 0$ first-order kinematic phase oscillators

$$\begin{aligned} M_i\ddot{\theta}_i + D_i\dot{\theta}_i &= \omega_i - \sum\nolimits_{j=1}^n a_{ij}\sin(\theta_i - \theta_j)\,, \qquad i \in \mathcal{V}_1, \\ D_i\dot{\theta}_i &= \omega_i - \sum\nolimits_{j=1}^n a_{ij}\sin(\theta_i - \theta_j)\,, \qquad i \in \mathcal{V}_2, \end{aligned} \tag{1}$$

where $\theta_i \in \mathbb{S}^1$ and $\dot{\theta}_i \in \mathbb{R}^1$ are the phase and frequency of oscillator $i \in \mathcal{V}$, $\omega_i \in \mathbb{R}^1$ and $D_i > 0$ are the natural frequency and damping coefficient of oscillator $i \in \mathcal{V}$, and $M_i > 0$ is inertial constant of oscillator $i \in \mathcal{V}_1$. The coupled oscillator model (1) evolves on $\mathbb{T}^n \times \mathbb{R}^{|\mathcal{V}_1|}$, and features an important symmetry, namely the rotational invariance of the angular variable θ. The interesting dynamics of the coupled oscillator model (1) arises from a competition between each oscillator's tendency to align with its natural frequency ω_i and the synchronization-enforcing coupling $a_{ij}\sin(\theta_i - \theta_j)$ with its neighbors.

As discussed in the main article, the coupled oscillator model (1) unifies various models proposed in the literature.

For example, for the parameters $\mathcal{V}_1 = \emptyset$ and $D_i = 1$ for all $i \in \mathcal{V}_2$, it reduces to the celebrated *Kuramoto model* [4, 5]

$$\dot{\theta}_i = \omega_i - \sum_{j=1}^{n} a_{ij} \sin(\theta_i - \theta_j)\,, \quad i \in \{1, \dots, n\}\,. \qquad [\mathbf{2}]$$

We refer to the review articles [6, 7, 8, 9, 10] for various theoretic results on the Kuramoto model [**2**] and further synchronization applications in natural sciences, technology, and social networks. Here, we present a detailed modeling of the spring oscillator network used as a mechanical analog in the main article, and we present a few power network models, which can be described by the coupled oscillator model [**1**].

Mechanical Spring Network. Consider the spring network illustrated in Figure 6 consisting of a group of n particles constrained to rotate around a circle with unit radius. For simplicity, we assume that the particles are allowed to move freely on the circle and exchange their order without collisions.

Each particle is characterized by its phase angle $\theta_i \in \mathbb{S}^1$ and frequency $\dot{\theta}_i \in \mathbb{R}$, and its inertial and damping coefficients are $M_i > 0$ and $D_i > 0$. The external forces and torques acting on each particle are (i) a viscous damping force $D_i\dot{\theta}_i$ opposing the direction of motion, (ii) a non-conservative force $\omega_i \in \mathbb{R}$ along the direction of motion depicting a preferred natural rotation frequency, and (iii) an elastic restoring torque between interacting particles i and j coupled by an ideal elastic spring with stiffness $a_{ij} > 0$ and zero rest length. The topology of the spring network is described by the weighted, undirected, and connected graph $G = (\mathcal{V}, \mathcal{E}, A)$.

To compute the elastic torque between the particles, we parametrize the position of each particle i by the unit vector $p_i = [\cos(\theta_i)\,, \sin(\theta_i)]^T \in \mathbb{S}^1 \subset \mathbb{R}^2$. The elastic Hookean energy stored in the springs is the function $E : \mathbb{T}^n \to \mathbb{R}$ given up to an additive constant by

$$\begin{aligned} E(\theta) &= \sum\nolimits_{\{i,j\}\in\mathcal{E}} \frac{a_{ij}}{2} \|p_i - p_j\|_2^2 \\ &= \sum\nolimits_{\{i,j\}\in\mathcal{E}} a_{ij} \big(1 - \cos(\theta_i)\cos(\theta_j) - \sin(\theta_i)\sin(\theta_j)\big) \\ &= \sum\nolimits_{\{i,j\}\in\mathcal{E}} a_{ij} \big(1 - \cos(\theta_i - \theta_j)\big)\,, \end{aligned}$$

where we employed the trigonometric identity $\cos(\alpha - \beta) = \cos\alpha\cos\beta + \sin\alpha\sin\beta$ in the last equality. Hence, we obtain the restoring torque acting on particle i as

$$T_i(\theta) = -\frac{\partial}{\partial\theta_i} E(\theta) = -\sum\nolimits_{j=1}^{n} a_{ij} \sin(\theta_i - \theta_j)\,.$$

Therefore, the network of spring-interconnected particles depicted in Figure 6 obeys the dynamics

$$M_i\ddot{\theta}_i + D_i\dot{\theta}_i = \omega_i - \sum\nolimits_{j=1}^{n} a_{ij} \sin(\theta_i - \theta_j)\,, \quad i \in \{1, \dots, n\}. \quad [\mathbf{3}]$$

In conclusion, the spring network in Figure 6 is a mechanical analog of the coupled oscillator model [**1**] with $\mathcal{V}_2 = \emptyset$.

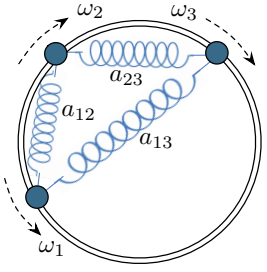

Fig. 6. Mechanical analog of the coupled oscillator model [**1**].

Power Network Model. The coupled oscillator model [**1**] includes also a variety of power network models. We briefly present different power network models compatible with the coupled oscillator model [**1**] and refer to [11, Chapter 7] for a detailed derivation from a higher order first principle model.

Consider a connected power network with generators $\mathcal{V}_1$ and load buses $\mathcal{V}_2$. The network is described by the symmetric nodal admittance matrix $Y \in \mathbb{C}^{n\times n}$ (augmented with the generator transient reactances). If the network is lossless and the voltage levels $|V_i|$ at all nodes $i \in \mathcal{V}_1 \cup \mathcal{V}_2$ are constant, then the *maximum real power transfer* between any two nodes $i, j \in \mathcal{V}_1 \cup \mathcal{V}_2$ is $a_{ij} = |V_i| \cdot |V_j| \cdot \Im(Y_{ij})$, where $\Im(Y_{ij})$ denotes the susceptance of the transmission line $\{i, j\} \in \mathcal{E}$. With this notation the swing dynamics of generator i are given by

$$M_i\ddot{\theta}_i + D_i\dot{\theta}_i = P_{\mathrm{m},i} - \sum\nolimits_{j=1}^{n} a_{ij} \sin(\theta_i - \theta_j)\,, \quad i \in \mathcal{V}_1, \quad [\mathbf{4}]$$

where $\theta_i \in \mathbb{S}^1$ and $\dot{\theta}_i \in \mathbb{R}^1$ are the generator rotor angle and frequency, $\theta_j \in \mathbb{S}^1$ for $j \in \mathcal{V}_2$ are the voltage phase angles at the load buses, and $P_{\mathrm{m},i} > 0$, $M_i > 0$, and $D_i > 0$ are the mechanical power input from the prime mover, the generator inertia constant, and the damping coefficient.

For the load buses $\mathcal{V}_2$, we consider the following three load models illustrated in Figure 7.

1) PV buses with frequency-dependent loads: All load buses are *PV buses*, that is, the active power demand $P_{\mathrm{l},i}$ and the voltage magnitude $|V_i|$ are specified for each bus. The real power drawn by load i consists of a constant term $P_{\mathrm{l},i} > 0$ and a frequency dependent term $D_i\dot{\theta}_i$ with $D_i > 0$, as illustrated in Figure 7(a). The resulting real power balance equation is

$$D_i\dot{\theta}_i + P_{\mathrm{l},i} = -\sum\nolimits_{j=1}^{n} a_{ij} \sin(\theta_i - \theta_j)\,, \quad i \in \mathcal{V}_2\,. \qquad [\mathbf{5}]$$

The dynamics [**4**]-[**5**] are known as *structure-preserving power network model* [12], and equal the coupled oscillator model [**1**] for $\omega_i = P_{\mathrm{m},i}$, $i \in \mathcal{V}_1$, and $\omega_i = -P_{\mathrm{l},i}$, $i \in \mathcal{V}_2$.

2) PV buses with constant power loads: All load buses are *PV buses*, each load features a constant real power demand $P_{\mathrm{l},i} > 0$, and the load damping in [**5**] is neglected, that is, $D_i = 0$ in equation [**5**]. The corresponding circuit-theoretic model is shown in Figure 7(b). If the angular distances $|\theta_i(t) - \theta_j(t)| < \pi/2$ are bounded for each transmission line $\{i, j\} \in \mathcal{E}$ (this condition will be precisely established in the next section), then the resulting differential-algebraic system has the same local stability properties as the dynamics [**4**]-[**5**], see [13]. Hence, all of our results apply locally also to the structure-preserving power network model [**4**]-[**5**] with zero load damping $D_i = 0$ for $i \in \mathcal{V}_2$.

3) Constant current and constant admittance loads: If each load $i \in \mathcal{V}_2$ is modeled as a constant current demand I_i and an (inductive) admittance $Y_{i,\mathrm{shunt}}$ to ground as illustrated in Figure 7(c), then the linear current-balance equations are $I = YV$, where $I \in \mathbb{C}^n$ and $V \in \mathbb{C}^n$ are the vectors of nodal current injections and voltages. After elimination of the bus variables V_i, $i \in \mathcal{V}_2$, through Kron reduction [3], the resulting dynamics assume the form [**3**] known as the (lossless) *network-reduced power system model* [14, 15]. We refer to [11, 3] for a detailed derivation of the network-reduced model.

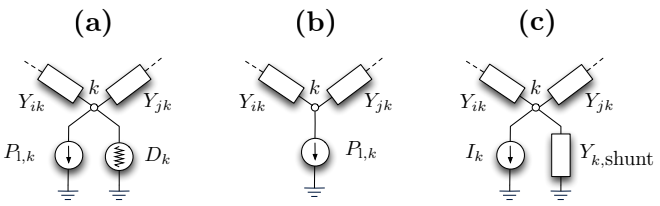

Fig. 7. Equivalent circuits of the frequency-dependent load model (a), the constant power load model (b), and the constant current and admittance load model (c).

The above model [4]-[5] is valid for an AC grid with synchronous generator and load models 1), 2), and 3). We remark that synchronous motor loads also assume the form [4] with $P_{\mathrm{m},i} < 0$ [16], and a first-principle modeling of a DC power source connected to an AC grid via a droop-controlled inverter results also in equation [5]; see [17] for further details.

Remark 1. (Voltage dynamics) To conclude this modeling paragraph, we want to state a word of caution regarding the load models. The PV load models 1) and 2) assume constant voltage magnitudes $|V_i|$ at the loads. Under normal operating conditions, the assumption of constant voltage magnitudes is well justified since voltage magnitudes are controlled at the generators, and the active power flow $a_{ij}\sin(\theta_i-\theta_j) = |V_i|\cdot|V_j|\cdot\Im(Y_{ij})\cdot\sin(\theta_i-\theta_j)$ between two nodes $i,j\in\mathcal{V}_1\cup\mathcal{V}_2$ is primarily governed by the angular difference $\theta_i-\theta_j$ and not by the voltage magnitudes $|V_i|,|V_j|$. The latter assumption is known as "decoupling assumption" in the power systems community. Whereas the model [4]-[5] is well-adopted for power systems stability studies, the assumption of constant load voltage magnitudes ceases to hold in a heavily stressed grid (near a bifurcation point), where additional dynamic phenomena can occur such as voltage collapse at the loads [18]. In short, the coupling weights a_{ij} are not necessarily constant.

Likewise, if the shunt admittance loads in the load model model 3) are not constant (e.g., constant power loads can be transformed to voltage-dependent shunt admittances), then the Kron reduction process may be ill-posed, or the admittance matrix of the network-reduced model depends on the load voltages. In the latter case, the coupling weights a_{ij} are again not constant but depend on the load voltages.

To explicitly account for such unmodeled voltage dynamics affecting the coupling weights a_{ij}, we study the coupled oscillator model [1] with interval-valued parameters in the section *Robust Synchronization in Presence of Uncertainty*.□

Synchronization Notions. The following subsets of the n-torus $\mathbb{T}^n$ are essential for the synchronization problem: For $\gamma\in[0,\pi/2[$, let $\bar{\Delta}_G(\gamma)\subset\mathbb{T}^n$ be the closed set of angle arrays $(\theta_1,\dots,\theta_n)$ with the property $|\theta_i-\theta_j|\leq\gamma$ for $\{i,j\}\in\mathcal{E}$. Also, let $\Delta_G(\gamma)$ be the interior of $\bar{\Delta}_G(\gamma)$.

Definition 1. *A solution* $(\theta,\dot\theta):\mathbb{R}_{\geq 0}\to(\mathbb{T}^n,\mathbb{R}^{|\mathcal{V}_1|})$ *to the coupled oscillator model* [1] *is said to be* synchronized *if* $\theta(0)\in\bar{\Delta}_G(\gamma)$ *and there exists* $\omega_{\mathrm{sync}}\in\mathbb{R}^1$ *such that* $\theta(t) = \theta(0)+\omega_{\mathrm{sync}}\mathbf{1}_n t \pmod{2\pi}$ *and* $\dot\theta(t)=\omega_{\mathrm{sync}}\mathbf{1}_{|\mathcal{V}_1|}$ *for all* $t\geq 0$.

In other words, here, synchronized trajectories have the properties of *frequency synchronization* and *phase cohesiveness*, that is, all oscillators rotate with the same synchronization frequency ω_{sync} and all their phases belong to the set $\bar{\Delta}_G(\gamma)$. For a power network model [4]-[5], the notion of phase cohesiveness is equivalent to bounded flows $|a_{ij}\sin(\theta_i-\theta_j)|\leq a_{ij}\sin(\gamma)$ for all transmission lines $\{i,j\}\in\mathcal{E}$.

For the coupled oscillator model [1], the explicit synchronization frequency is given by $\omega_{\mathrm{sync}}\triangleq\sum_{i=1}^n\omega_i/\sum_{i=1}^n D_i$, see [9] for a detailed derivation. By transforming to a rotating frame with frequency ω_{sync} and by replacing ω_i by $\omega_i - D_i\omega_{\mathrm{sync}}$, we obtain $\omega_{\mathrm{sync}}=0$ (or equivalently $\omega\in\mathbf{1}_n^\perp$) corresponding to balanced power injections $\sum_{i\in\mathcal{V}_1}P_{\mathrm{m},i} = \sum_{i\in\mathcal{V}_2}P_{\mathrm{l},i}$ in power network applications. Hence, without loss of generality, we assume that $\omega\in\mathbf{1}_n^\perp$ such that $\omega_{\mathrm{sync}}=0$.

Given a point $r\in\mathbb{S}^1$ and an angle $s\in[0,2\pi]$, let $\mathrm{rot}_s(r)\in\mathbb{S}^1$ be the rotation of r counterclockwise by the angle s. For $(r_1,\dots,r_n)\in\mathbb{T}^n$, define the equivalence class

$$[(r_1,\dots,r_n)] = \{(\mathrm{rot}_s(r_1),\dots,\mathrm{rot}_s(r_n))\in\mathbb{T}^n \mid s\in[0,2\pi]\}.$$

Clearly, if $(r_1,\dots,r_n)\in\bar{\Delta}_G(\gamma)$, then $[(r_1,\dots,r_n)]\subset\bar{\Delta}_G(\gamma)$.

Definition 2. *Given* $\theta\in\bar{\Delta}_G(\gamma)$ *for some* $\gamma\in[0,\pi/2[$, *the set* $([\theta],\mathbf{0}_{|\mathcal{V}_1|})\subset\mathbb{T}^n\times\mathbb{R}^{|\mathcal{V}_1|}$ *is a* synchronization manifold *of the coupled oscillator model* [1].

Note that a synchronized solution takes value in a synchronization manifold due to rotational symmetry. For two first-order oscillators [2] the state space $\mathbb{T}^2$, the set $\Delta_G(\pi/2)$, as well as the synchronization manifold $[\theta^*]$ associated to an angle array $\theta^*=(\theta_1^*,\theta_2^*)\in\mathbb{T}^2$ are illustrated in Figure 8.

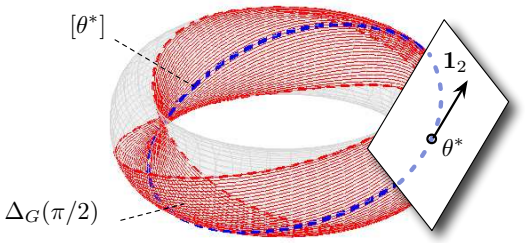

Fig. 8. Illustration of the state space $\mathbb{T}^2$, the set $\Delta_G(\pi/2)$, the synchronization manifold $[\theta^*]$ associated to a point $\theta^*=(\theta_1^*,\theta_2^*)\in\Delta_G(\pi/2)$, the tangent space at θ^*, and the translation vector $\mathbf{1}_2$.

Existing Synchronization Conditions. The coupled oscillator dynamics [1], and the Kuramoto dynamics [2] for that matter, feature (i) the synchronizing effect of the coupling described by the weighted edges of the graph $G(\mathcal{V},\mathcal{E},A)$ and (ii) the de-synchronizing effect of the dissimilar natural frequencies $\omega\in\mathbf{1}_n^\perp$ at the nodes. Loosely speaking, synchronization occurs when the coupling dominates the dissimilarity. Various conditions are proposed in the power systems and synchronization literature to quantify this tradeoff between coupling and dissimilarity. The coupling is typically quantified by the algebraic connectivity $\lambda_2(L)$ [19, 15, 20, 21, 22, 23] or the weighted nodal degree $\deg_i\triangleq\sum_{j=1}^n a_{ij}$ [24, 3, 25, 15, 26], and the dissimilarity is quantified by either absolute norms $\|\omega\|_p$ or incremental (relative) norms $\|B^T\omega\|_p$, where typically $p\in\{2,\infty\}$. Sometimes, these conditions can be evaluated only numerically since they are state-dependent [19, 24] or arise from a non-trivial linearization process, such as the Master stability function formalism [22, 23, 27]. In general, concise and accurate results are only known for specific topologies such as complete graphs [9, 28] linear chains [29, 30] and complete bipartite graphs [31] with uniform weights.

For arbitrary coupling topologies only sufficient conditions are known [19, 15, 20, 24] as well as numerical investigations for random networks [32, 21, 33, 34]. To best of our knowledge, the sharpest and provably correct synchronization conditions for arbitrary topologies assume the form $\lambda_2(L) > \left(\sum_{\{i,j\}\in\mathcal{E}}|\omega_i-\omega_j|^2\right)^{1/2}$, see [10, Theorem 4.7]. For arbitrary undirected, connected, and weighted, graphs $G(\mathcal{V},\mathcal{E},A)$, simulation studies indicate that the known sufficient conditions [19, 15, 20, 24] are conservative estimates on

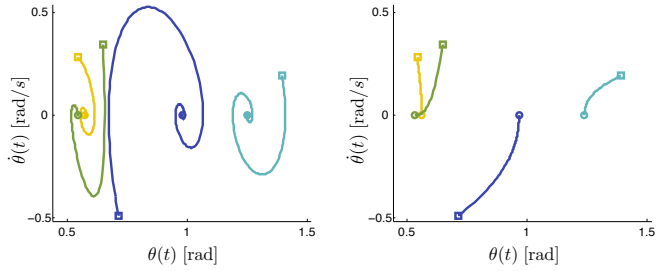

Fig. 9. The left plot shows the phase space dynamics of a network of $n = 4$ second-order oscillators [3] with $\mathcal{V}_2 = \emptyset$ and Kuramoto-type coupling $a_{ij} = K/n$ for all distinct $i, j \in \mathcal{V}_1 = \{1, \dots, 4\}$ and for $K \in \mathbb{R}$. The right plot shows the phase space dynamics corresponding to first-order Kuramoto oscillators [2] together with the frequency dynamics $\frac{d}{dt}\dot\theta = -M^{-1}D\dot\theta$. The natural frequencies ω_i and the coupling strength K are chosen such that $\omega_{\text{sync}} = 0$ and $K = 1.1 \cdot \max_{i,j\in\{1,\dots,4\}} |\omega_i - \omega_j|$. From the same initial configuration $\theta(0)$ (denoted by ■) both first and second-order oscillators converge exponentially to the same synchronized equilibria (denoted by ●), as predicted by Lemma 1.

the threshold from incoherence to synchrony, and every review article on synchronization concludes with the open problem of finding sharp synchronization conditions [7, 9, 6, 22, 23, 35].

Mathematical Analysis of Synchronization

This section presents our analysis of the synchronization problem in the coupled oscillator model [1].

An Algebraic Approach to Synchronization. Here we present a novel analysis approach that reduces the synchronization problem to an equivalent algebraic problem that reveals the crucial role of cycles and cut-sets in the graph topology. In a first analysis step, we reduce the synchronization problem for the coupled oscillator model [1] to a simpler problem, namely stability of a first-order model. It turns out that existence and local exponential stability of synchronized solutions of the coupled oscillator model [1] can be entirely described by means of the first-order Kuramoto model [2].

Lemma 1. (Synchronization equivalence) *Consider the coupled oscillator model* [1] *and the Kuramoto model* [2]. *The following statements are equivalent for any* $\gamma \in [0, \pi/2[$ *and any synchronization manifold* $([\theta], \mathbf{0}_{|\mathcal{V}_1|}) \subset \bar\Delta_G(\gamma) \times \mathbb{R}^{|\mathcal{V}_1|}$.

(i) $[\theta]$ *is a locally exponentially stable synchronization manifold of the Kuramoto model* [2]*; and*
(ii) $([\theta], \mathbf{0}_{|\mathcal{V}_1|})$ *is a locally exponentially stable synchronization manifold of the coupled oscillator model* [1].

If the equivalent statements (i) and (ii) are true, then, locally near their respective synchronization manifolds, the coupled oscillator model [1] *and the Kuramoto model* [2] *together with the frequency dynamics* $\frac{d}{dt}\dot\theta = -M^{-1}D\dot\theta$ *are topologically conjugate.*

Loosely speaking, the topological conjugacy result means that the trajectories of the two plots in Figure 4 can be continuously deformed to match each other while preserving parameterization of time. Lemma 1 is illustrated in Figure 4, and its proof can be found in [9, Theorems 5.1 and 5.3].

By Lemma 1, the local synchronization problem for the coupled oscillator model [1] reduces to the synchronization problem for the first-order Kuramoto model [2]. Henceforth, we restrict ourselves to the Kuramoto model [2]. The following result is known in the synchronization literature [20, 15] as well as in power systems, where the saturation of a transmission line is corresponds to a singularity of the load flow Jacobian resulting in a saddle node bifurcation [36, 37, 13, 12, 38, 39, 24, 19, 40, 41, 18, 42].

Lemma 2. (Stable synchronization in $\bar\Delta_G(\pi/2)$) *Consider the Kuramoto model* [2] *with a connected graph* $G(\mathcal{V}, \mathcal{E}, A)$, *and let* $\gamma \in [0, \pi/2[$. *The following statements hold:*

1) **Jacobian:** *The Jacobian of the Kuramoto model evaluated at* $\theta \in \mathbb{T}^n$ *is given by*

$$J(\theta) = -B\,\mathrm{diag}(\{a_{ij}\cos(\theta_i - \theta_j)\}_{\{i,j\}\in\mathcal{E}})B^T\,;$$

2) **Stability:** *If there exists an equilibrium point* $\theta^* \in \bar\Delta_G(\gamma)$, *then it belongs to a locally exponentially stable equilibrium manifold* $[\theta^*] \in \bar\Delta_G(\gamma)$*; and*
3) **Uniqueness:** *This equilibrium manifold is unique in* $\bar\Delta_G(\gamma)$.

Proof Since we have that $\frac{\partial}{\partial\theta_i}\big(\omega_i - \sum_{k=1}^n a_{ik}\sin(\theta_i - \theta_k)\big) = -\sum_{k=1}^n a_{ik}\cos(\theta_i - \theta_k)$ and $\frac{\partial}{\partial\theta_j}\big(\omega_i - \sum_{k=1}^n a_{ik}\sin(\theta_i - \theta_k)\big) = a_{ij}\cos(\theta_i - \theta_j)$, the negative Jacobian of the right-hand side of the Kuramoto model [2] equals the Laplacian matrix of the connected graph $G(\mathcal{V}, \mathcal{E}, \tilde A)$ where $\tilde a_{ij} = a_{ij}\cos(\theta_i - \theta_j)$. Equivalently, in compact notation the Jacobian is given by $J(\theta) = -B\,\mathrm{diag}(\{a_{ij}\cos(\theta_i - \theta_j)\}_{\{i,j\}\in\mathcal{E}})B^T$. This completes the proof of statement 1).

The Jacobian $J(\theta)$ evaluated at an equilibrium point $\theta^* \in \bar\Delta_G(\gamma)$ is negative semidefinite with rank $n-1$. Its nullspace is $\mathbf{1}_n$ and arises from the rotational symmetry of the right-hand side of the Kuramoto model [2], see Figure 8 for an illustration. Consequently, the equilibrium point $\theta^* \in \bar\Delta_G(\gamma)$ is locally (transversally) exponentially stable. Moreover, the corresponding equilibrium manifold $[\theta^*] \in \bar\Delta_G(\gamma)$ is locally exponentially stable. This completes the proof of statement 2).

To prove statement 3), we denote the right-hand side of [2] by $f : \mathbb{T}^n \to \mathbb{R}^n$, where f is defined component-wise by

$$f_i(\theta) = \omega_i - \sum\nolimits_{j=1}^n a_{ij}\sin(\theta_i - \theta_j)\,, \quad i \in \{1, \dots, n\}\,.$$

In [39, Corollary 1], it is shown that $f - \omega$ is a one-to-one function on $\bar\Delta_G(\pi/2)$ modulo rotational symmetry, that is, for $\theta_1 \in \bar\Delta_G(\pi/2)$ and $\theta_2 \in \bar\Delta_G(\pi/2)$, we have that $f(\theta_1) = f(\theta_2)$ if and only if $[\theta_1] = [\theta_2]$. This proves uniqueness of the equilibrium manifold in $\bar\Delta_G(\gamma)$, $\gamma \in [0, \pi/2[$. ■

By Lemma 2, the problem of finding a locally stable synchronization manifold reduces to that of finding a fixed point $\theta^* \in \bar\Delta_G(\gamma)$ for some $\gamma \in [0, \pi/2[$. The fixed-point equations of the Kuramoto model [2] read as

$$\omega_i = \sum\nolimits_{j=1}^n a_{ij}\sin(\theta_i - \theta_j)\,, \quad i \in \{1, \dots, n\}\,. \qquad [6]$$

In a compact notation the fixed-point equations [6] are

$$\omega = B\,\mathrm{diag}\left(\{a_{ij}\}_{\{i,j\}\in\mathcal{E}}\right)\mathbf{sin}(B^T\theta)\,. \qquad [7]$$

The following conditions show that the natural frequencies ω have to be absolutely and incrementally bounded and the nodal degree has to be sufficiently large such that fixed points of [6] exist.

Lemma 3. (Necessary synchronization conditions) *Consider the Kuramoto model* [2] *with graph* $G(\mathcal{V}, \mathcal{E}, A)$ *and* $\omega \in \mathbf{1}_n^\perp$. *Let* $\gamma \in [0, \pi/2[$, *and define the weighted nodal degree* $\deg_i \triangleq \sum_{j=1}^n a_{ij}$ *for each node* $i \in \{1, \dots, n\}$. *The following statements hold:*

1) **Absolute boundedness:** *If there exists a synchronized solution* $\theta \in \bar\Delta_G(\gamma)$, *then*

$$\deg_i \sin(\gamma) \geq |\omega_i| \qquad \text{for all } i \in \{1, \dots, n\}\,. \qquad [8]$$

2) **Incremental boundedness:** *If there exists a synchronized solution $\theta \in \bar{\Delta}_G(\gamma)$, then*

$$(\deg_i + \deg_j)\sin(\gamma) \geq |\omega_i - \omega_j| \qquad \text{for all } \{i,j\} \in \mathcal{E}\,. \quad [9]$$

Proof The first condition arises since $\sin(\theta_i - \theta_j) \in [-\sin(\gamma), \sin(\gamma)]$ for $\theta \in \bar{\Delta}_G(\gamma)$, and the fixed-point equation [6] has no solution if condition [8] is not satisfied.

Alternatively, since $\omega \in \mathbf{1}_n^\perp$, a multiplication of the fixed point equation [7] by the vector $(e_i^n - e_j^n) \in \mathbf{1}_n^\perp$, for $\{i,j\} \in \mathcal{E}$, or equivalently a subtraction of the ith and jth fixed-point equation [6], yields the following equation for all $\{i,j\} \in \mathcal{E}$:

$$\omega_i - \omega_j = \sum\nolimits_{k=1}^{n} \left(a_{ik}\sin(\theta_i - \theta_k) - a_{jk}\sin(\theta_j - \theta_k)\right)\,. \quad [10]$$

Again, equation [10] has no solution in $\bar{\Delta}_G(\gamma)$ if condition [9] is not satisfied. ∎

In the following we aim to find sufficient and sharp conditions under which the fixed-point equations [7] admit a solution $\theta^* \in \bar{\Delta}_G(\gamma)$. We resort to a rather straightforward solution ansatz. By formally replacing each term $\sin(\theta_i - \theta_j)$ in the fixed-point equations [7] by an auxiliary scalar variable ψ_{ij}, the fixed-point equation [7] is equivalently written as

$$\omega = B\,\mathrm{diag}\left(\{a_{ij}\}_{\{i,j\}\in\mathcal{E}}\right)\,\psi\,, \quad [11]$$

$$\psi = \mathbf{sin}(B^T\theta)\,, \quad [12]$$

where $\psi \in \mathbb{R}^{|\mathcal{E}|}$ is a vector with elements ψ_{ij}. We will refer to equations [11] as the *auxiliary-fixed point equation*, and characterize their properties in the following theorem.

Theorem 1. (Properties of the fixed point equations) *Consider the Kuramoto model [2] with graph $G(\mathcal{V},\mathcal{E},A)$ and $\omega \in \mathbf{1}_n^\perp$, its fixed-point equations [7], and the auxiliary fixed-point equations [11]. The following statements hold:*

1) **Exact solution:** *Every solution of the auxiliary fixed-point equations [11] is of the form*

$$\psi = B^T L^\dagger \omega + \psi_{\mathrm{hom}}\,, \quad [13]$$

where the homogeneous solution $\psi_{\mathrm{hom}} \in \mathbb{R}^{|\mathcal{E}|}$ satisfies $\mathrm{diag}\left(\{a_{ij}\}_{\{i,j\}\in\mathcal{E}}\right)\,\psi_{\mathrm{hom}} \in \mathrm{Ker}\,(B)$.

2) **Exact synchronization condition:** *Let $\gamma \in [0, \pi/2[$. The following three statements are equivalent:*

(i) There exists a solution $\theta^* \in \bar{\Delta}_G(\gamma)$ to the fixed-point equation [7];

(ii) There exists a solution $\theta \in \bar{\Delta}_G(\gamma)$ to

$$B^T L^\dagger \omega + \psi_{\mathrm{hom}} = \mathbf{sin}(B^T\theta)\,. \quad [14]$$

for some $\psi_{\mathrm{hom}} \in \mathrm{diag}\left(\{1/a_{ij}\}_{\{i,j\}\in\mathcal{E}}\right)\ker(B)$; and

(iii) There exists a solution $\psi \in \mathbb{R}^{|\mathcal{E}|}$ to the auxiliary fixed-point equation [11] of the form [13] satisfying the norm constraint $\|\psi\|_\infty \leq \sin(\gamma)$ and the cycle constraint $\mathbf{arcsin}(\psi) \in \mathrm{Im}\,(B^T)$.

If the three equivalent statements (i), (ii), and (iii) are true, then we have the identities $B^T\theta^* = B^T\theta = \mathbf{arcsin}(\psi)$. Additionally, $[\theta^*] \in \bar{\Delta}_G(\gamma)$ is a locally exponentially stable synchronization manifold.

Proof *Statement 1):* Every solution $\psi \in \mathbb{R}^{|\mathcal{E}|}$ to the auxiliary fixed-point equations [11] is of the form $\psi = \psi_{\mathrm{hom}} + \psi_{\mathrm{pt}}$, where ψ_{hom} is the homogeneous solution and ψ_{pt} is a particular solution. The homogeneous solution satisfies $B\,\mathrm{diag}\left(\{a_{ij}\}_{\{i,j\}\in\mathcal{E}}\right)\psi_{\mathrm{hom}} = \mathbf{0}_n$. One can easily verify that $\psi_{\mathrm{pt}} = B^T L^\dagger \omega$ is a particular solution[1], since $B\,\mathrm{diag}(\{a_{ij}\}_{\{i,j\}\in\mathcal{E}})\psi_{\mathrm{pt}} = B\,\mathrm{diag}(\{a_{ij}\}_{\{i,j\}\in\mathcal{E}})B^T L^\dagger\omega = LL^\dagger\omega = \left(I_n - \frac{1}{n}\mathbf{1}_{n\times n}\right)\omega = \omega$.

Statement 2), equivalence $\big((\mathrm{i}) \Leftrightarrow (\mathrm{ii})\big)$: If there exists a solution θ^* of the fixed-point equations [7], then θ^* can be equivalently obtained from equation [12] together with the solution [13] of the auxiliary equations [11]. These two equations directly give equation [14].

Equivalence $\big((\mathrm{ii}) \Leftrightarrow (\mathrm{iii})\big)$: For $\theta^* \in \bar{\Delta}_G(\gamma)$, we have from equation [14] that $\|\psi\|_\infty \leq \sin(\gamma)$ and $\mathbf{arcsin}(\psi) = B^T\theta^*$, that is, $\mathbf{arcsin}(\psi) \in \mathrm{Im}\,(B^T)$. Conversely, if the norm constraint $\|\psi\|_\infty \leq \sin(\gamma)$ and the cycle constraint $\mathbf{arcsin}(\psi) \in \mathrm{Im}\,(B^T)$ are met, then equation [14] is solvable in $\bar{\Delta}_G(\gamma)$, that is, there is $\theta^* \in \bar{\Delta}_G(\gamma)$ such that $\mathbf{arcsin}(\psi) = B^T\theta^*$. The local exponential stability of the associated synchronization manifold $[\theta^*]$ follows then directly from Lemma 2. ∎

The particular solution $B^T L^\dagger \omega$ to the auxiliary fixed-point equations [11] lives in the cut-set space $\mathrm{Ker}\,(B)^\perp$ and the homogenous solution ψ_{hom} lives in the weighted cycle space $\psi_{\mathrm{hom}} \in \mathrm{diag}\left(\{1/a_{ij}\}_{\{i,j\}\in\mathcal{E}}\right)\mathrm{Ker}\,(B)$. As a consequence, by statement (iii) of Theorem 1, for each cycle in the graph, we obtain one degree of freedom in choosing the homogeneous solution ψ_{hom} as well as one nonlinear constraint $c^T\,\mathbf{arcsin}(\psi) = 0$, where $c \in \ker(B)$ is a signed path vector corresponding to the cycle.

Remark 2. (Comments on necessity) The cycle space $\mathrm{Ker}\,(B)$ of the graph serves as a degree of freedom to find a minimum ∞-norm solution ψ^* to equations [11] via

$$\min\nolimits_{\psi\in\mathbb{R}^{|\mathcal{E}|}} \|\psi\|_\infty \quad \text{subject to} \quad \omega = B\,\mathrm{diag}\left(\{a_{ij}\}_{\{i,j\}\in\mathcal{E}}\right)\,\psi. \quad [15]$$

By Theorem 1, such a minimum ∞-norm solution ψ^* necessarily satisfies $\|\psi^*\|_\infty \leq \sin(\gamma)$ so that an equilibrium $\theta^* \in \bar{\Delta}_G(\gamma)$ exists. Hence, the condition $\|\psi^*\|_\infty \leq \sin(\gamma)$ is an *optimal necessary synchronization condition.*

The optimization problem [15] – the minimum ∞-norm solution to an under-determined and consistent system of linear equations – is well studied in the context of kinematically redundant manipulators. Its solution is known to be non-unique and contained in a disconnected solution space [43, 44]. Unfortunately, there is no "a priori" analytic formula to construct a minimum ∞-norm solution, but the optimization problem is computationally tractable via its dual problem $\max_{u\in\mathbb{R}^n} u^T\omega$ subject to $\|\,\mathrm{diag}\left(\{a_{ij}\}_{\{i,j\}\in\mathcal{E}}\right)\,B^T u\|_1 = 1$. □

Synchronization Assessment for Specific Networks. In this subsection we seek to establish that the condition

$$\boxed{\left\|B^T L^\dagger \omega\right\|_\infty = \left\|L^\dagger\omega\right\|_{\mathcal{E},\infty} < 1} \quad [16]$$

is sufficient for the existence of locally exponentially stable equilibria in $\Delta_G(\pi/2)$. More general, for a given level of phase cohesiveness $\gamma \in [0, \pi/2[$ we seek to establish that the condition

$$\boxed{\left\|B^T L^\dagger \omega\right\|_\infty = \left\|L^\dagger\omega\right\|_{\mathcal{E},\infty} \leq \sin(\gamma)} \quad [17]$$

is sufficient for the existence of locally exponentially stable equilibria in $\bar{\Delta}_G(\gamma)$. Since the right-hand side of [17] is a

[1] Likewise, it can also be shown that $(B\,\mathrm{diag}(\{a_{ij}\}_{\{i,j\}\in\mathcal{E}}))^\dagger\omega$ as well as $\mathrm{diag}(\{a_{ij}\}_{\{i,j\}\in\mathcal{E}})^{-1}B^\dagger\omega$ are other possible particular solutions. All of these solutions differ only by addition of a homogenous solution. Each one can be interpreted as solution to a weighted least squares problem, see [43]. Further solutions can also be constructed in a graph-theoretic way by a spanning-tree decomposition, see [2]. Our specific choice $\psi_{\mathrm{pt}} = B^T L^\dagger\omega$ has the property that $\psi_{\mathrm{pt}} \in \mathrm{Im}\,(B^T)$ lives in the cut-set space, and it is the most useful particular solution in order to proceed with our synchronization analysis.

concave function of $\gamma \in [0, \pi/2[$ that achieves its supremum value at $\gamma^* = \pi/2$, it follows that condition [17] implies [16].

In the main article, we provide a detailed interpretation of the synchronization conditions [16] and [17] from various practical perspectives. Before continuing our theoretical analysis, we provide two further abstract but insightful perspectives on the conditions [16] and [17].

Remark 3. (Interpretation of the sync condition) *Graph-theoretic interpretation:* With regards to the exact and state-dependent norm and cycle conditions in statement (iii) of Theorem 1, the proposed condition [17] is simply a norm constraint on the network parameters in cut-set space $\mathrm{Im}\,(B^T)$ of the graph topology, and cycle components are discarded.

Circuit-theoretic interpretation: In a circuit or power network, the variable $\omega \in \mathbb{R}^n$ corresponds to nodal power injections. Let $x \in \mathbb{R}^{|\mathcal{E}|}$ satisfy $Bx = \omega$, then x corresponds to equivalent power injections along lines $\{i,j\} \in \mathcal{E}$.[2] Condition [16] can then be rewritten as $\left\|B^T L^\dagger B x\right\|_\infty < 1$. The matrix $B^T L^\dagger B \in \mathbb{R}^{|\mathcal{E}|\times|\mathcal{E}|}$ has elements $(e_n^i - e_n^j)^T L^\dagger (e_n^k - e_n^\ell)$ for $\{i,j\},\{k,\ell\} \in \mathcal{E}$, its diagonal elements are the effective resistances R_{ij}, and its off-diagonal elements are the network distribution (sensitivity) factors [45, Appendix 11A]. Hence, from a circuit-theoretic perspective condition [16] restricts the pair-wise effective resistances and the routing of power through the network similar to the resistive synchronization conditions developed in [24, 3, 25] □

As it turns out, the exact state-dependent synchronization conditions in Theorem 1 can be easily evaluated for the sparsest (acyclic) and densest (homogeneous) topologies and for "worst-case" (cut-set inducing) and "best" (identical) natural frequencies. For all of these cases the scalar condition [17] is sharp. To quantify a "sharp" condition in the following theorem, we distinguish between *exact* (necessary and sufficient) conditions and *tight* conditions, which are sufficient in general and become necessary over a set of parametric realizations.

Theorem 2. (Sync condition for extremal network topologies and parameters) *Consider the Kuramoto model* [2] *with connected graph* $G(\mathcal{V},\mathcal{E},A)$ *and* $\omega \in \mathbf{1}_n^\perp$. *Consider the inequality condition* [17] *for* $\gamma \in [0,\pi/2[$. *The following statements hold:*

(G1) **Exact synchronization condition for acyclic graphs:** *Assume that* $G(\mathcal{V},\mathcal{E},A)$ *is acyclic. There exists a locally exponentially stable equilibrium* $\theta^* \in \bar{\Delta}_G(\gamma)$ *if and only if condition* [17] *holds. Moreover, in this case we have that* $B^T\theta^* = \mathbf{arcsin}(B^T L^\dagger \omega) \in \bar{\Delta}_G(\gamma)$;

(G2) **Tight synchronization condition for homogeneous graphs:** *Assume that* $G(\mathcal{V},\mathcal{E},A)$ *is a homogeneous graph, that is, there is* $K > 0$ *such that* $a_{ij} = K$ *for all distinct* $i,j \in \{1,\dots,n\}$. *Consider a compact interval* $\Omega \subset \mathbb{R}$, *and let* $\mathbf{\Omega} = (\mathbf{\Omega}_1,\dots,\mathbf{\Omega}_n) \subset \mathbb{R}^n$ *be the set of all vectors with components* $\mathbf{\Omega}_i \in \Omega$ *for all* $i \in \{1,\dots,n\}$. *For all* $\omega \in \mathbf{\Omega}$ *there exists a locally exponentially stable equilibrium* $\theta^* \in \bar{\Delta}_G(\gamma)$ *if and only if condition* [17] *holds;*

(G3) **Exact synchronization condition for cut-set inducing natural frequencies:** *Let* $\Omega_1, \Omega_2 \in \mathbb{R}$, *and let* $\mathbf{\Omega} = (\mathbf{\Omega}_1,\dots,\mathbf{\Omega}_n) \subset \mathbb{R}^n$ *be the set of bipolar vectors with components* $\mathbf{\Omega}_i \in \{\Omega_1,\Omega_2\}$ *for* $i \in \{1,\dots,n\}$. *For all* $\omega \in L\mathbf{\Omega}$ *there exists a locally exponentially stable equilibrium* $\theta^* \in \bar{\Delta}_G(\gamma)$ *if and only if condition* [17] *holds. Moreover,* $\mathbf{\Omega}$ *induces a cut-set: if* $|\Omega_2 - \Omega_1| = \sin(\gamma)$, *then for any particular* $\mathbf{\Omega}^* \in \mathbf{\Omega}$ *and* $\omega = L\mathbf{\Omega}^*$ *we obtain the equilibrium* $\theta^* \in \bar{\Delta}_G(\gamma)$ *satisfying* $B^T\theta^* = \mathbf{arcsin}(B^T\mathbf{\Omega}^*)$, *that is, for all* $\{i,j\} \in \mathcal{E}$, $|\theta_i^* - \theta_j^*| = 0$ *if* $\mathbf{\Omega}_i^* = \mathbf{\Omega}_j^*$ *and* $|\theta_i^* - \theta_j^*| = \gamma$ *if* $\mathbf{\Omega}_i^* \neq \mathbf{\Omega}_j^*$; *and*

(G4) **Asymptotic correctness:** *In the limit* $\|B^T L^\dagger \omega\|_\infty \to 0$, *that is, for identical natural frequencies and/or asymptotically strong network coupling, there is a locally exponentially stable equilibrium* θ^* *satisfying*

$$\lim_{\|B^T L^\dagger \omega\|_\infty \to 0} \frac{(B^T\theta^*)_i}{(\mathbf{arcsin}(B^T L^\dagger \omega))_i} = 1\,, \quad i \in \{1,\dots,|\mathcal{E}|\}\,.$$

Proof *Statement (G1):* For an acyclic graph we have that $\mathrm{Ker}\,(B) = \emptyset$. According to Theorem 1, there exists an equilibrium $\theta^* \in \bar{\Delta}_G(\gamma)$ if and only if condition [17] is satisfied. In this case, we obtain $B^T\theta^* = \mathbf{arcsin}(B^T L^\dagger \omega)$. This completes the proof of statement (G1).

Statement (G2): In the homogeneous case, we have that $L = K\big(nI_n - \mathbf{1}_{n\times n}\big)$ and $L^\dagger = \frac{1}{Kn}\big(I_n - \frac{1}{n}\mathbf{1}_{n\times n}\big)$, see [3, Lemma 3.13]. Thus, the inequality condition [17] can be equivalently rewritten as $\sin(\gamma) \geq \left\|B^T L^\dagger \cdot \omega\right\|_\infty = \frac{1}{Kn}\left\|B^T\omega\right\|_\infty$. According to [9, Theorem 4.1], the Kuramoto model [2] with homogenous coupling $a_{ij} = K$ features an exponentially stable equilibrium $\theta^* \in \bar{\Delta}_G(\gamma)$, $\gamma \in [0,\pi/2[$, for all $\omega \in \mathbf{\Omega}$ if and only if the condition $K > \left\|B^T\omega\right\|_\infty / n$ is satisfied. This concludes the proof of statement (G2).

Statement (G3): For notational convenience, let $c \triangleq \Omega_1 - \Omega_2$. Then, for any $\mathbf{\Omega}^* \in \mathbf{\Omega}$ and for $\omega = L\mathbf{\Omega}^*$, we have that $B^T L^\dagger \omega = B^T L^\dagger L \mathbf{\Omega}^* = B^T\mathbf{\Omega}^*$ is a vector with components $\{-c, 0, +c\}$. Now consider the solution $\psi = B^T L^\dagger \omega = B^T\mathbf{\Omega}^*$ to the auxiliary fixed point equations [11], and notice that $\mathbf{arcsin}(\psi) = \mathbf{arcsin}(B^T\mathbf{\Omega}^*)$ has components $\{-\arcsin(c), 0, +\arcsin(c)\}$. In particular, we have that $\mathbf{arcsin}(\psi) \in \mathrm{Im}\,(B^T)$, and the exact synchronization condition from Theorem 1 is satisfied if and only if $\|\psi\|_\infty = c \leq \sin(\gamma)$, which corresponds to condition [17]. The cut-set property follows since $B^T\theta^* = \mathbf{arcsin}(\psi)$ has components $\{-\arcsin(c), 0, +\arcsin(c)\} = \{-\gamma, 0, +\gamma\}$. This concludes the proof of statement (G3).

Statement (G4): Since $\arcsin(x)/x = 1 + x^2/6 + \mathcal{O}(x)^4$, we have that $(\mathbf{arcsin}(B^T L^\dagger\omega))_i / (B^T L^\dagger\omega)_i = 1 + \mathcal{O}((B^T L^\dagger\omega)_i^2)$ for each component $i \in \{1,\dots,|\mathcal{E}|\}$. Thus, in the limit $B^T L^\dagger\omega \to \mathbf{0}_{|\mathcal{E}|}$, it follows that $\mathbf{arcsin}(B^T L^\dagger\omega) \in \mathrm{Im}\,(B^T)$, and the cycle constraint $\mathbf{arcsin}(\psi) = \mathbf{arcsin}(B^T L^\dagger\omega + \psi_{\mathrm{hom}}) \in \mathrm{Im}\,(B^T)$ is met with $\psi_{\mathrm{hom}} = \mathbf{0}_{|\mathcal{E}|}$. For $B^T L^\dagger\omega \to \mathbf{0}_{|\mathcal{E}|}$ the norm constraint $\|B^T L^\dagger\omega\|_\infty \leq \sin(\gamma)$ is satisfied as well with $\gamma \searrow 0$, and we obtain[3] for each $i \in \{1,\dots,|\mathcal{E}|\}$ that

$$\lim_{B^T L^\dagger\omega \to \mathbf{0}_{|\mathcal{E}|}} \big(B^T\theta^*\big)_i / \big(\mathbf{arcsin}(B^T L^\dagger\omega)\big)_i = 1\,.$$

This concludes the proof of statement (G4) and Theorem 2. ■

Theorem 1 shows that the solvability of the fixed-point equations [7] is inherently related to the *cycle constraints*. The following lemma establishes feasibility of a single cycle.

Lemma 4. (Single cycle feasibility) *Consider the Kuramoto model* [2] *with a cycle graph* $G(\mathcal{V},\mathcal{E},A)$ *and* $\omega \in \mathbf{1}_n^\perp$. *Without loss of generality, assume that the edges are labeled by* $\{i, i+1\} \pmod n$ *for* $i \in \{1,\dots,n\}$ *and* $\mathrm{Ker}\,(B) = \mathrm{span}(\mathbf{1}_n)$. *Define* $x \in \mathbf{1}_n^\perp$ *and* $y \in \mathbb{R}^n_{>0}$ *uniquely by* $x \triangleq B^T L^\dagger\omega$ *and* $y_i \triangleq a_{i,(i+1) \pmod n} > 0$ *for* $i \in \{1,\dots,n\}$. *Let* $\gamma \in [0,\pi/2[$. *The following statements are equivalent:*

(i) There exists a locally exponentially stable equilibrium $\theta^* \in \bar{\Delta}_G(\gamma)$; *and*

[2] Notice that x is not uniquely determined if the circuit features loops.

[3] The limit $\|B^T L^\dagger\omega\|_\infty \to 0$ implies that the resulting equilibrium $\theta^* \in \bar{\Delta}_G(0)$ corresponds to phase synchronization $\theta_i = \theta_j$ for all $i,j \in \{1,\dots,n\}$. The converse statement $\theta^* \in \bar{\Delta}_G(0) \implies \omega = \mathbf{0}_n$ is also true and its proof can be found in [9, Theorem 5.5].

(ii) The function $f:[\lambda_{\min},\lambda_{\max}]\to\mathbb{R}$ with domain boundaries $\lambda_{\min}=\max_{i\in\{1,\dots,n\}}\frac{-\sin(\gamma)-x_i}{y_i}$ and $\lambda_{\max}=\min_{i\in\{1,\dots,n\}}\frac{\sin(\gamma)-x_i}{y_i}$ and defined by $f(\lambda)=\sum_{i=1}^n\arcsin(x_i+\lambda y_i)$ satisfies $f(\lambda_{\min})<0<f(\lambda_{\max})$.

If both equivalent statements 1) and 2) are true, then $B^T\theta^*=\mathbf{arcsin}(x+\lambda^* y)$, where $\lambda^*\in[\lambda_{\min},\lambda_{\max}]$ satisfies $f(\lambda^*)=0$.

Proof According to Theorem 1, there exists a locally exponentially stable equilibrium $\theta^*\in\bar{\Delta}_G(\gamma)$ if and only if there exists a solution $\psi=x+\lambda y$, $\lambda\in\mathbb{R}$, to the auxiliary fixed-point equations [**11**] satisfying the norm constraint $\|\psi\|_\infty\le\sin(\gamma)$ and the cycle constraint $\mathbf{arcsin}(\psi)\in\mathrm{Im}\,(B^T)$.

Equivalently, since $\mathrm{Ker}\,(B)=\mathrm{span}(\mathbf{1}_n)$, there is $\lambda\in\mathbb{R}$ satisfying the norm constraint $\|x+\lambda y\|_\infty\le\sin(\gamma)<1$ and the cycle constraint $\mathbf{1}_n^T\mathbf{arcsin}(x+y\lambda)=0$. Equivalently, the function $f(\lambda)=\mathbf{1}_n^T\mathbf{arcsin}(x+y\lambda)$ features a zero $\lambda^*\in[\lambda_{\min},\lambda_{\max}]$ (corresponding to the cycle constraint), where the constraints on $\lambda_{\min}$ and $\lambda_{\max}$ guarantee the norm constraints $x_i+y_i\lambda_{\max}\le\sin(\gamma)$ and $x_i+y_i\lambda_{\min}\ge-\sin(\gamma)$ for all $i\in\{1,\dots,n\}$. Equivalently, by the intermediate value theorem and due to continuity and (strict) monotonicity of the function f, we have that $f(\lambda_{\min})<0<f(\lambda_{\max})$. Finally, if $\lambda^*\in[\lambda_{\min},\lambda_{\max}]$ is found such that $f(\lambda^*)=0$, then, by Theorem 1, $B^T\theta^*=\mathbf{arcsin}(\psi)=\mathbf{arcsin}(x+\lambda^* y)$. ∎

Lemma 4 offers a checkable synchronization condition for cycles, which leads to the following theorem.

Theorem 3. (Sync conditions for cycle graphs) *Consider the Kuramoto model* [**2**] *with a cycle graph $G(\mathcal{V},\mathcal{E},A)$ and $\omega\in\mathbf{1}_n^\perp$. Consider the inequality condition* [**17**] *for $\gamma\in[0,\pi/2[$. The following statements hold.*

(C1) **Exact sync condition for symmetric natural frequencies:** *Assume that $\omega\in\mathbf{1}_n^\perp$ is such that $B^TL^\dagger\omega$ is a symmetric vector [4]. There is a locally exponentially stable equilibrium $\theta^*\in\bar{\Delta}_G(\gamma)$ if and only if condition* [**17**] *holds. Moreover, in this case $B^T\theta^*=\mathbf{arcsin}(B^TL^\dagger\omega)$.*

(C2) **Tight sync condition for low-dimensional cycles:** *Assume the network contains $n\in\{3,4\}$ oscillators. Consider a compact interval $\Omega\subset\mathbb{R}$, and let $\mathbf{\Omega}=(\mathbf{\Omega}_1,\dots,\mathbf{\Omega}_n)\subset\mathbb{R}^n$ be the set of vectors with components $\mathbf{\Omega}_i\in\Omega$ for all $i\in\{1,\dots,n\}$. For all $\omega\in L\mathbf{\Omega}$ there exists a locally exponentially stable equilibrium $\theta^*\in\bar{\Delta}_G(\gamma)$ if and only if condition* [**17**] *holds.*

(C3) **General cycles and network parameters:** *In general for $n\ge5$ oscillators, condition* [**16**] *does not guarantee existence of an equilibrium $\theta^*\in\Delta_G(\pi/2)$. As a sufficient condition, there exists a locally exponentially stable equilibrium $\theta^*\in\bar{\Delta}_G(\gamma)$, $\gamma\in[0,\pi/2[$, if*

$$\left\|B^TL^\dagger\omega\right\|_\infty\le\frac{\min_{\{i,j\}\in\mathcal{E}}a_{ij}}{\max_{\{i,j\}\in\mathcal{E}}a_{ij}+\min_{\{i,j\}\in\mathcal{E}}a_{ij}}\cdot\sin(\gamma)\,.\quad[\mathbf{18}]$$

Proof To prove the statements of Theorem 3 and to show the existence of an equilibrium $\theta^*\in\bar{\Delta}_G(\gamma)$, we invoke the equivalent formulation via the function $f(\lambda)$ as constructed in Lemma 4. In particular, we seek to prove the statement:

> Let $\lambda_{\min}=\max_{i\in\{1,\dots,n\}}\frac{-\sin(\gamma)-x_i}{y_i}$ and $\lambda_{\max}=\min_{i\in\{1,\dots,n\}}\frac{\sin(\gamma)-x_i}{y_i}$. The function $f:[\lambda_{\min},\lambda_{\max}]\to\mathbb{R}$ defined by $f(\lambda)=\sum_{i=1}^n\arcsin(x_i+\lambda y_i)$ satisfies $f(\lambda_{\min})<0<f(\lambda_{\max})$ (equivalently there is $\lambda^*\in[\lambda_{\min},\lambda_{\max}]$ such that $f(\lambda^*)=0$) if and only if the condition $\|x\|_\infty=\|B^TL^\dagger\omega\|_\infty\le\sin(\gamma)$ is satisfied.

Statement (C1): For a symmetric vector $x=B^TL^\dagger\omega$, all odd moments about the (zero) mean vanish, that is, $\sum_{i=1}^n x_i^{2p+1}=0$ for $p\in\mathbb{N}_0$. Since the Taylor series of the arcsin about zero features only odd powers, we have $f(0)=\sum_{i=1}^n\arcsin(x_i)=\sum_{i=1}^n\sum_{p=0}^\infty\frac{(2p)!}{2^{2p}(p!)^2(2p+1)}x_i^{2p+1}=0$. Statement 1) follows then immediately from Lemma 4.

Statement (C2): By statement (C1), statement (C2) is true if $B^TL^\dagger\omega$ is symmetric. Statement (C2), can then be proved in a combinatorial fashion by considering all deviations from symmetry arising for three or four oscillators. In order to continue recall that $\arcsin(x)$ is a super-additive function for $x\in[0,1]$ and a sub-additive function for $x\in[-1,0]$, that is, $\arcsin(x)+\arcsin(y)<\arcsin(x+y)$ for $x,y>0$ and $x+y\le1$, $\arcsin(x)+\arcsin(y)>\arcsin(x+y)$ for $x,y<0$ and $x+y\ge-1$, and $\arcsin(x)+\arcsin(y)=\arcsin(x+y)$ for $x=y=0$. We now consider each case $n\in\{3,4\}$ separately.

Proof of sufficiency for $n=3$: Assume that $\|x\|_\infty\le\sin(\gamma)$. Since the case $f(\lambda=0)=\mathbf{1}_n^T\mathbf{arcsin}(x)=0$ for a symmetric vector $x\in\mathbb{R}^3$ is already proved, we consider now the asymmetric case $f(\lambda=0)=\mathbf{1}_n^T\mathbf{arcsin}(x)>0$ (the proof of the case $\mathbf{1}_n^T\mathbf{arcsin}(x)<0$ is analogous). Necessarily, it follows that at least two elements of x are negative: if one element of x is zero, say $x_1=0$, then we fall back into the symmetric case $x_2=-x_3$; on the other hand, if only one element is negative, say $x_1<0$ and $x_2,x_3>0$, then we arrive at a contradiction since $f(\lambda=0)=\sum_{i=1}^n\arcsin(x_i)=-\arcsin(x_2+x_3)+\arcsin(x_2)+\arcsin(x_3)<0$ due to super-additivity and since $x_1=-x_2-x_3$. Hence, without loss of generality, let $x=[a+b,-a,-b]^T$ where $a,b>0$. By assumption $\|x\|_\infty\le\sin(\gamma)$. It follows that $a+b\le\sin(\gamma)$, $a<\sin(\gamma)$, $b<\sin(\gamma)$, and $\lambda_{\min}=\max_{i\in\{1,\dots,n\}}\frac{-\sin(\gamma)-x_i}{y_i}<0$.

Due to super-additivity, $f(\lambda=0)=\mathbf{1}_n^T\mathbf{arcsin}(x)=\arcsin(a+b)-(\arcsin(a)+\arcsin(b))>0$. Now we evaluate $f(\lambda)$ at the lower end of its domain $[\lambda_{\min},\lambda_{\max}]$ and obtain

$$\begin{aligned}f(\lambda_{\min})=\;&\arcsin(a+b+y_1\lambda_{\min})+\arcsin(-a+y_2\lambda_{\min})\\&+\arcsin(-b+y_3\lambda_{\min})\,.\end{aligned}\quad[\mathbf{19}]$$

By the definition of $\lambda_{\min}$, at least one summand on the right-hand side of [**19**] equals $-\gamma$. Furthermore, notice that the second and the third summand are negative, and the first summand satisfies $\arcsin(a+b+y_1\lambda_{\min})\ge-\gamma$. If $\arcsin(a+b+y_1\lambda_{\min})=-\gamma$, then clearly $f(\lambda_{\min})<0$. In the other case, $\arcsin(a+b+y_1\lambda_{\min})>-\gamma$, it follows that

$$\begin{aligned}f(\lambda_{\min})<\;&\underbrace{\arcsin(a+b+y_1\lambda_{\min})-\gamma}_{<0}\\&+\underbrace{\max\{\arcsin(-a+y_2\lambda_{\min}),\arcsin(-b+y_3\lambda_{\min})\}}_{<0}<0\,.\end{aligned}$$

Since $f(\lambda_{\min})<0<f(0)\le f(\lambda_{\max})$, it follows from Lemma 4 that there exists a stable equilibrium $\theta^*\in\bar{\Delta}_G(\gamma)$. The sufficiency is proved for $n=3$.

Proof of sufficiency for $n=4$: Assume that $\|x\|_\infty\le\sin(\gamma)$. Without loss of generality, let $\mathrm{argmax}_{i\in\{1,\dots,4\}}\{|x_i|\}$ be a singleton (otherwise x is necessarily symmetric), and let $x\in\mathbf{1}_n^\perp$ be such that $f(\lambda=0)=\mathbf{1}_n^T\mathbf{arcsin}(x)>0$ (the proof of the case $\mathbf{1}_n^T\mathbf{arcsin}(x)<0$ is analogous). Necessarily, it follows that at least two elements of x are negative: if only one element of x is negative, say $x_1<0$ and $x_2,x_3,x_4\ge0$, then we

[4] A vector $x\in\mathbf{1}_n^\perp$ is *symmetric* if its histogram is symmetric, that is, up to permutation of its elements, x is of the form $x=[-c,+c]^T$ for n even and some vector $c\in\mathbb{R}^{n/2}$ and $x=[-c,0,+c]^T$ for n odd and some $c\in\mathbb{R}^{(n-1)/2}$.

arrive at a contradiction since $f(\lambda=0)=\sum_{i=1}^n \arcsin(x_i) = -\arcsin(x_2+x_3+x_4)+\arcsin(x_2)+\arcsin(x_3)+\arcsin(x_4)$ is zero only in the symmetric case (for example, $x_2=x_3=0<x_4=-x_1$) and strictly negative otherwise (due to super-additivity). If exactly one element of x is positive (and three are non-postive), say $x=[a+b+c,-a,-b,-c]^T$ for $a,b,c\geq 0$ and $a+b+c=\|x\|_\infty \leq \sin(\gamma)$, then, an analogous reasoning to the case $n=3$ leads to $f(\lambda_{\min})<0$.

It remains to consider the case of two positive and two negative entries. Without loss of generality let $x_1\geq x_2>0>x_3\geq x_4$, where $x_1\neq -x_4$ and $x_2\neq -x_3$ (this is the symmetric case), $\sum_{i=1}^n x_i=0$, and $\|x\|_\infty\leq \sin(\gamma)$ by assumption. It follows that $\lambda_{\min}=\max_{i\in\{1,\dots,n\}}\frac{-\sin(\gamma)-x_i}{y_i}\leq 0$. Since $f(\lambda=0)=\mathbf{1}_n^T\arcsin(x)>0$ and $\mathbf{1}_n^T x=0$, it follows from super-additivity that $\|x\|_\infty=\max\{x_1,x_2\}$, and the set $\operatorname{argmax}\{x_1,x_2\}$ must be a singleton (otherwise we arrive again at a contradiction or at the symmetric case). Suppose that $\|x\|_\infty=\max\{x_1,x_2\}=x_1$, then necessarily $|x_2|<|x_3|\leq|x_4|<|x_1|\leq\sin(\gamma)$. It follows that $\lambda_{\min}<0$.

Again, we evaluate the sum $f(\lambda_{\min})=\sum_{i=1}^4\arcsin(x_i+y_i\lambda_{\min})$. Notice that the last two summands $\arcsin(x_3+y_3\lambda_{\min})$ and $\arcsin(x_4+y_4\lambda_{\min})$ are negative (since $0>x_3\geq x_4$ and $\lambda_{\min}<0$), and the first two summands satisfy $\min\{\arcsin(x_1+y_1\lambda_{\min}),\arcsin(x_2+y_2\lambda_{\min})\}\geq-\gamma$. If $\min\{\arcsin(x_1+y_1\lambda_{\min}),\arcsin(x_2+y_2\lambda_{\min})\}=-\gamma$, we have

$$f(\lambda_{\min})=\underbrace{\arcsin(x_3+y_3\lambda_{\min})+\arcsin(x_4+y_4\lambda_{\min})}_{<0}$$
$$+\underbrace{\big(-\gamma+\max\{\arcsin(x_1+y_1\lambda_{\min}),\arcsin(x_2+y_2\lambda_{\min})\}\big)}_{<0}<0.$$

In case that $\min\{\arcsin(a+y_1\lambda_{\min}),\arcsin(b+y_2\lambda_{\min})\}>-\gamma$, we obtain $\min_{i\in\{3,4\}}\{\arcsin(x_i+y_i\lambda_{\min})\}=-\gamma$ and

$$f(\lambda_{\min})<\arcsin(x_1+y_1\lambda_{\min})+\arcsin(x_2+y_2\lambda_{\min})-\gamma + \max_{i\in\{3,4\}}\{\arcsin(x_i+y_i\lambda_{\min})\}.$$

Since $|x_2|<|x_3|\leq|x_4|<|x_1|\leq\sin(\gamma)$, it readily follows that $\arcsin(x_1+y_1\lambda_{\min})-\gamma<0$ and $\arcsin(x_2+y_2\lambda_{\min})+\max_{i\in\{3,4\}}\{\arcsin(x_i+y_i\lambda_{\min})\}<0$. We conclude that $f(\lambda_{\min})<0$. Since $f(\lambda_{\min})<0<f(0)\leq f(\lambda_{\max})$, it follows from Lemma 4 that there exists a stable equilibrium $\theta^*\in\bar\Delta_G(\gamma)$. The sufficiency is proved for $n=4$.

Proof of necessity for $n\in\{3,4\}$: We prove the necessity by contradiction. Consider a compact cube $\mathcal{Q}=[-c,+c]^{|\mathcal{E}|}\subset\mathbb{R}^{|\mathcal{E}|}$, where $c>0$ satisfies $c>\sin(\gamma)$. Assume that for every $x\in\mathbf{1}_n^\perp$, even those satisfying $\|x\|_\infty\geq c$, there exists $\lambda\in\mathbb{R}$ such that the cycle constraint $\mathbf{1}_n^T\,\mathbf{arcsin}(x+\lambda y)=0$ and the norm constraint $\|x+\lambda y\|_\infty\leq\sin(\gamma)$ are simultaneously satisfied. For the sake of contradiction, consider now the symmetric case, where $x\in\mathbf{1}_n^\perp$ has components $x_i\in\{-c,+c,0\}$. As proved in statement (C1), $\lambda^*=0$ uniquely solves the cycle constraint equation $0=f(\lambda^*=0)=\sum_{i=1}^n\arcsin(x_i+\lambda^* y)=\sum_{i=1}^n\arcsin(\pm c)$ for any value of $c\in[0,1]$. However, the norm constraint $\|x+\lambda^* y\|_\infty=\|x\|_\infty\leq\sin(\gamma)$ can be satisfied only if $\|x\|_\infty\leq\sin(\gamma)<c$. We arrive at a contradiction since we assumed $\|x\|_\infty\geq c>\sin(\gamma)$.

We conclude that, if $x=B^TL^\dagger\omega$ is bounded within a compact cube $\mathcal{Q}=[-c,+c]^{|\mathcal{E}|}\subset\mathbb{R}^{|\mathcal{E}|}$ with $c\leq\sin(\gamma)$, the condition [**17**] is also necessary for synchronization of all considered parametric realizations of $B^TL^\dagger\omega$ within this compact cube $\mathcal{Q}$. For the compact set $\mathbf{\Omega}=\Omega^n\subset\mathbb{R}^n$, it follows that the image $B^TL^\dagger\cdot L\mathbf{\Omega}=B^T\mathbf{\Omega}$ equals the compact cube $\mathcal{Q}=\big[-\big(\max_{\omega\in\Omega}\omega-\min_{\omega\in\Omega}\omega\big),+\big(\max_{\omega\in\Omega}\omega-\min_{\omega\in\Omega}\omega\big)\big]^{|\mathcal{E}|}$. Hence, the condition [**17**] is necessary for synchronization of all considered parametric realizations of ω in the compact set $L\mathbf{\Omega}$. This concludes the proof of statement (C2).

Statement (C3): To prove the first part of statement (C3) we construct an explicit counterexample. Consider a cycle of length $n\geq 5$ with unit-weighed edges $a_{i,i+1}=1$, and let

$$\omega=\alpha\cdot\big[1+\tfrac{1}{n-3}\quad 0\quad -2\quad 1-\tfrac{1}{n-3}\quad \mathbf{0}_{n-4}\big]^T,$$

where $\alpha\in[0,1]$. For $\alpha<1$, these parameters satisfy the necessary conditions [**8**] and [**9**]. For the given parameters, we obtain the non-symmetric vector $x=B^TL^\dagger\omega$ given by

$$x=B^TL^\dagger\omega=\alpha\cdot\big[-1\quad -1\quad 1\quad \tfrac{1}{n-3}\mathbf{1}_{(n-3)}\big]^T. \qquad [\mathbf{20}]$$

Notice that $\|x\|_\infty=\alpha<1$, x is non-symmetric, and x is the minimum ∞-norm vector $\psi=x+\lambda\mathbf{1}_n$ for $\lambda\in\mathbb{R}$.

In the following, we will show that there exists no equilibrium in $\lim_{\gamma\uparrow\pi/2}\bar\Delta_G(\gamma)=\bar\Delta_G(\pi/2)$. Consider the function $f(\lambda)=\mathbf{arcsin}(\mathbf{1}_n^Tx+\lambda\mathbf{1}_n)$ whose domain is centered symmetrically around zero, that is, $\lambda_{\max}=-\lambda_{\min}=\lim_{\gamma\uparrow\pi/2}(\sin(\gamma)-\alpha)=1-\alpha$. Notice that the domain of f vanishes as $\alpha\uparrow 1$. For $n\to\infty$ we have that $\lim_{n\to\infty}f(0)=-\arcsin(\alpha)+\lim_{n\to\infty}(n-3)\cdot\arcsin(\alpha/(n-3))=-\arcsin(\alpha)+\alpha$. Hence, as $n\to\infty$ and $\alpha\uparrow 1$, we obtain $f(0)=-\frac{\pi}{2}+1<0$. Due to continuity of f with respect to α,n,λ, we conclude that for $n\geq 5$ sufficiently large and $\alpha<1$ sufficiently large, there is no λ^* such that $f(\lambda^*)=0$. Hence, the condition $\|x\|_\infty=\|B^TL^\dagger\omega\|_\infty<1$ does generally not guarantee existence of $\theta^*\in\bar\Delta_G(\pi/2)\supset\Delta_G(\pi/2)$. A second numerical counterexample will be constructed in Example 1 below.

A sufficient condition for the existence of an equilibrium $\theta^*\in\Delta_G(\gamma)$ is $x_i+\lambda_{\min}y_i\leq 0\leq x_i+\lambda_{\max}y_i$ for each $i\in\{1,\dots,n\}$, which is equivalent to condition [**18**]. Indeed if condition [**18**] holds, we obtain $f(\lambda_{\min})=\sum_{i=1}^n\arcsin(x_i+\lambda_{\min}y_i)$ as a sum of nonpositive terms and $f(\lambda_{\max})=\sum_{i=1}^n\arcsin(x_i+\lambda_{\max}y_i)$ as a sum of nonnegative terms. Since $\mathbf{1}_n^Tx=0$ and generally $x\neq\mathbf{0}_n$ (otherwise we fall back in the symmetric case), at least one x_i is strictly negative and at least one x_i is strictly positive, and it follows that $f(\lambda_{\min})<0<f(\lambda_{\max})$. The statement (C3) follows then immediately from Lemma 4. This concludes the proof. ∎

In the following, define a *patched network* $\{G(\mathcal{V},\mathcal{E},A),\omega\}$ as a collection of subgraphs and natural frequencies $\omega\in\mathbf{1}_n^\perp$, where *(i)* each subgraph is connected, *(ii)* in each subgraph one of the conditions (G1),(G2),(G3),(G4), (C1), or (C2) is satisfied, *(iii)* the subgraphs are connected to another through edges $\{i,j\}\in\mathcal{E}$ satisfying $\|(e_i^{|\mathcal{E}|}-e_j^{|\mathcal{E}|})^TL^\dagger\omega\|_\infty\leq\sin(\gamma)$, and *(iv)* the set of cycles in the overall graph $G(\mathcal{V},\mathcal{E},A)$ is equal to the union of the cycles of all subgraphs. Since a patched network satisfies the synchronization condition [**17**] as well the norm and cycle constraints, we can state the following result.

Corollary 4. (Sync condition for a patched network) *Consider the Kuramoto model* [**2**] *with a patched network* $\{G(\mathcal{V},\mathcal{E},A),\omega\}$*, and let* $\gamma\in[0,\pi/2[$*. There is a locally exponentially stable equilibrium* $\theta^*\in\bar\Delta_G(\gamma)$ *if condition* [**17**] *holds.*

Example 1. (Numerical cyclic counterexample and its intuition) In the proof of Theorem 3, we provided an analytic counterexample which demonstrates that condition [**17**] is not sufficiently tight for synchronization in sufficiently large cyclic networks. Here, we provide an additional numerical counterexample. Consider a cycle family of length $n=5+3\cdot p$, where $p\in\mathbb{N}_0$ is a nonnegative integer. Without loss of generality, assume that the edges are labeled by $\{i,i+1\}\pmod n$

for $i \in \{1,\dots,n\}$ such that $\mathrm{Ker}\,(B) = \mathrm{span}(\mathbf{1}_n)$. Assume that all edges are unit-weighed $a_{i,i+1 \pmod n} = 1$ for $i \in \{1,\dots,n\}$. Consider $\alpha \in [0,1[$, and let

$$\omega = \alpha \cdot \begin{bmatrix} -1/2 & 2 & \mathbf{0}_{p+1} & 3/2 & \mathbf{0}_{2p+1} \end{bmatrix}^T .$$

For $n = 5$ ($p = 1$) the graph and the network parameters are illustrated in Figure . For the given network parameters, we obtain the non-symmetric vector $B^T L^\dagger \omega$ given by

$$B^T L^\dagger \omega = \alpha \cdot \begin{bmatrix} 1 & -1 & -\mathbf{1}_{(n-2)/3} & 1/2 \cdot \mathbf{1}_{2(n-2)/3} \end{bmatrix}^T .$$

Analogously to the example provided in the proof of Theorem 3, $\|B^T L^\dagger \omega\|_\infty = \alpha$ and $B^T L^\dagger \omega$ is the minimum ∞-norm vector $B^T L^\dagger \omega + \lambda \mathbf{1}_n$ for $\lambda \in \mathbb{R}$. In the limit $\alpha \uparrow 1$, the necessary condition [**8**] is satisfied with equality. In Figure , for $\alpha \uparrow 1$, we have that $\omega_2 = 2$, and the necessary condition [**8**] reads as $a_{12} + a_{23} = |\omega_2| = 2$, and the corresponding equilibrium equation $\sin(\theta_1 - \theta_2) + \sin(\theta_3 - \theta_2) = 2$ can only be satisfied if $\theta_1 - \theta_2 = \pi/2$ and $\theta_3 - \theta_2 = \pi/2$. Thus, with two fixed edge differences there is no more "wiggle room" to compensate for the effects of ω_i, $i \in \{1,3,4,5\}$. As a consequence, there is no equilibrium $\theta^* \in \bar{\Delta}_G(\pi/2)$ for $\alpha = 1$ or equivalently $\|B^T L^\dagger \omega\|_\infty = 1$. Due to continuity of the equations [**6**] with respect to α, we conclude that for $\alpha < 1$ sufficiently large there is no equilibrium either. Numerical investigations show that this conclusion is true, especially for very large cycles. For the extreme case $p = 10^7$, we obtain the critical threshold $\alpha \approx 0.9475$ where $\theta^* \in \bar{\Delta}_G(\pi/2)$ ceases to exist. □

Notice that both the counterexample used in the proof of Theorem 3 and the one in Example 1 are at the boundary of the admissible parameter space, where the necessary condition [**8**] is marginally satisfied. In the next section, we establish that such "degenerate" counterexamples do almost never occur for generic network topologies and parameters.

To conclude this section, we remark that the main technical difficulty in proving sufficiency of the condition [**17**] for arbitrary graphs is the compact state space $\mathbb{T}^n$ and the non-monotone sinusoidal coupling among the oscillators. Indeed, if the state space was $\mathbb{R}^n$ and if the oscillators were coupled via non-decreasing and odd functions, then the synchronization problem simplifies tremendously and the counterexamples in the proof of Theorem 3 and in Example 1 do not occur; see [46] for an elegant analysis based on optimization theory.

Robust Synchronization in Presence of Uncertainty

In order to evaluate the synchronization condition [**17**], all network parameters a_{ij} and ω_i need to be known exactly. In many applications, this global knowledge is an unrealistic assumptions, the network parameters may be uncertain, or even not constant over time. For instance, in power networks, the load and generation profiles $P_{\mathrm{m},i}$ and $P_{\mathrm{l},i}$ as well as the voltage magnitudes $|V_i|$ may be known only with a certain degree of accuracy, they have underlying unmodeled (or even unknown) dynamics, and they can be regarded as constant only over short time intervals. Hence, the associated natural frequencies ω_i and the coupling weights $a_{ij} = |V_i| \cdot |V_j| \cdot \Im(Y_{ij})$ are known only within certain ranges, and a synchronization test should be robust with respect to parametric variations.

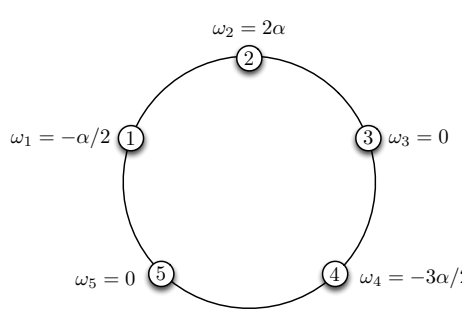

Fig. 10. Cycle graph with $n = 5$ nodes and non-symmetric choice of ω.

In the following, we take parametric uncertainties into account and extend the synchronization condition [**17**] to interval-valued network parameters. We consider a set of interval-valued natural frequencies defined by

$$\mathbf{\Omega} = \left\{ \omega \in \mathbf{1}_n^\perp : \underline{\omega_i} \le \omega_i \le \overline{\omega_i} \ \ \forall\, i \in \{1,\dots,n\} \right\},$$

that is, for a vector $\omega \in \mathbf{\Omega}$ each entry is subject to upper and lower bounds. Accordingly, consider a set of edge weights defined by the interval-valued adjacency matrix[5]

$$\mathcal{A} = \Big\{ A \in \mathbb{R}^{n\times n} : 0 < \underline{a_{ij}} \le a_{ij} = a_{ji} \le \overline{a_{ij}} \ \ \forall\, \{i,j\} \in \mathcal{E}\,, \\ a_{ij} = a_{ji} = 0 \ \forall\, \{i,j\} \notin \mathcal{E} \Big\}.$$

Notice that both $\mathbf{\Omega}$ and $\mathcal{A}$ are convex sets and simply hypercubes in the vector spaces $\mathbf{1}_n^\perp$ and $\mathbb{R}^{n\times n}$. We define the associated discrete sets of vertices of $\mathbf{\Omega}$ and $\mathcal{A}$ by

$$\mathrm{vert}(\mathbf{\Omega}) = \left\{ \omega \in \mathbf{1}_n^\perp : \omega_i \in \{\underline{\omega_i}, \overline{\omega_i}\} \ \ \forall\, i \in \{1,\dots,n\} \right\},$$

$$\mathrm{vert}(\mathcal{A}) = \Big\{ A \in \mathbb{R}^{n\times n} : a_{ij} = a_{ji} \in \{\underline{a_{ij}}, \overline{a_{ij}}\} \ \ \forall\, \{i,j\} \in \mathcal{E}\,, \\ a_{ij} = a_{ji} = 0 \ \forall\, \{i,j\} \notin \mathcal{E} \Big\}.$$

Accordingly, consider the associated interval-valued Laplacian

$$\mathcal{L} = \left\{ L \in \mathbb{R}^{n\times n} : L = \mathrm{diag}\big(\{\textstyle\sum_{j=1}^n a_{ij}\}_{i=1}^n\big) - A\,, A \in \mathcal{A} \right\}$$

and its discrete vertex set

$$\mathrm{vert}(\mathcal{L}) = \Big\{ L \in \mathbb{R}^{n\times n} : L = \mathrm{diag}\big(\{\textstyle\sum_{j=1}^n a_{ij}\}_{i=1}^n\big) - A\,, \\ A \in \mathrm{vert}(\mathcal{A}) \Big\}.$$

In the following, denote the convex hull of a set $\mathcal{S}$ by $\mathrm{conv}(\mathcal{S})$. By construction, we have that $\mathbf{\Omega} = \mathrm{conv}(\mathrm{vert}(\mathbf{\Omega}))$, $\mathcal{A} = \mathrm{conv}(\mathrm{vert}(\mathcal{A}))$, and $\mathcal{L} = \mathrm{conv}(\mathrm{vert}(\mathcal{L}))$.

Next, we consider a connected interval-valued network $\{G(\mathcal{V},\mathcal{E},\mathcal{A})\,,\,\omega\}$ with $A \in \mathcal{A}$ and $\omega \in \mathbf{\Omega}$. Consider the associated *interval-valued Laplacian equation*

$$Lx = \omega\,, \qquad [\mathbf{21}]$$

where $x \in \mathbf{1}_n^\perp$ is a variable and $L \in \mathcal{L}$ and $\omega \in \mathbf{\Omega}$ are parameters. The set of solutions $x \in \mathcal{X}$ to [**21**] is given by

$$\mathcal{X} = \left\{ x \in \mathbf{1}_n^\perp : x = L^\dagger \omega\,, L \in \mathcal{L}\,, \omega \in \mathbf{\Omega} \right\}.$$

Accordingly, define the associated discrete vertex set

$$\mathrm{vert}(\mathcal{X}) = \\ \left\{ x \in \mathbf{1}_n^\perp : x = L^\dagger \omega\,, L \in \mathrm{vert}(\mathcal{L})\,, \omega \in \mathrm{vert}(\mathbf{\Omega}) \right\}.$$

The following lemma for interval-valued linear systems is known for non-singular and interval-valued M-matrices [47] and circuit-tableau matrices [48, 49]. To best of our knowledge this result is unknown for Laplacian matrices (corresponding to singular M-matrices or circuit-tableau matrices).

[5] The following analysis can be easily extended to the case of zero edge weights implying a non-constant edge set $\mathcal{E}$ as long as the associated graph remains connected. Since the resulting notation is cumbersome, and since the combinatorial insights are not very surprising, we omit it here.

Lemma 5. (Interval-valued Laplacian equations) *Consider the interval-valued Laplacian equation* [**21**]*. The set of solutions $\mathcal{X}$ is contained in the convex hull of its vertex set* $\mathrm{vert}(\mathcal{X})$*, that is,* $\mathrm{conv}(\mathcal{X}) = \mathrm{conv}(\mathrm{vert}(\mathcal{X}))$.

Proof We first analyze the interval-valued Laplacian equation [**21**] for the case that $\mathbf{\Omega}$ is a singleton, that is, we consider a fixed value of $\omega \in \mathbf{1}_n^\perp$ and parametric variations of $L \in \mathcal{L}$. By [3, Lemma III.9], we have for any Laplacian L corresponding to a connected, undirected, and weighted graph and for any arbitrary constant $\delta \neq 0$ that

$$(L + (\delta/n)\,\mathbf{1}_{n\times n})^{-1} = L^\dagger + (1/\delta n)\,\mathbf{1}_{n\times n}\,,$$

Consequently, for any $L \in \mathcal{L}$ and $\omega \in \mathbf{1}_n^\perp$, we have that

$$\begin{aligned} x = L^\dagger\omega &= \big(L^\dagger + (1/\delta n)\,\mathbf{1}_{n\times n}\big)\omega \\ &= (L + (\delta/n)\,\mathbf{1}_{n\times n})^{-1}\,\omega \\ &= \Big(\underbrace{\textstyle\sum_{\{i,j\}\in\mathcal{E}} a_{ij}(e_i^n - e_j^n)\cdot(e_i^n - e_j^n)^T + (\delta/n)\,\mathbf{1}_n\mathbf{1}_n^T}_{=Q}\Big)^{-1}\omega\,. \end{aligned}$$

Thus, $x \in \mathbf{1}_n^\perp$ is the solution to the equation $Qx = \omega$, where Q is a regular interval-valued matrix, and each parametric variation $0 < \underline{a_{ij}} \leq a_{ij} = a_{ji} \leq \overline{a_{ij}}$, $\{i,j\} \in \mathcal{E}$ enters additively via a rank-one matrix. Hence, the regularity assumptions of the interval-valued analyses in [48, Theorem 1] and [49, Theorem 4.2] are satisfied, and we conclude that $\mathrm{conv}(\mathcal{X}) = \mathrm{conv}(\mathrm{vert}(\mathcal{X}))$.

Next, consider the case that $\mathcal{L}$ is a singleton, that is, we consider only variations of $\omega \in \mathbf{\Omega}$. Recall that $L^\dagger$ is a Laplacian matrix corresponding to a connected, undirected, and weighted graph [3]. Let the edge weights of this graph be denoted by $\tilde{a}_{ij} = \tilde{a}_{ji} \geq 0$. Hence, for any $\omega \in \mathbf{\Omega}$, we obtain

$$x = L^\dagger\omega = \begin{bmatrix} \sum_{j=1}^n \tilde{a}_{1j}(\omega_1 - \omega_j) \\ \vdots \\ \sum_{j=1}^n \tilde{a}_{nj}(\omega_n - \omega_j) \end{bmatrix} \preceq \begin{bmatrix} \sum_{j=1}^n \tilde{a}_{1j}(\overline{\omega_1} - \underline{\omega_j}) \\ \vdots \\ \sum_{j=1}^n \tilde{a}_{nj}(\overline{\omega_n} - \underline{\omega_j}) \end{bmatrix},$$

$$x = L^\dagger\omega = \begin{bmatrix} \sum_{j=1}^n \tilde{a}_{1j}(\omega_1 - \omega_j) \\ \vdots \\ \sum_{j=1}^n \tilde{a}_{nj}(\omega_n - \omega_j) \end{bmatrix} \succeq \begin{bmatrix} \sum_{j=1}^n \tilde{a}_{1j}(\underline{\omega_1} - \overline{\omega_j}) \\ \vdots \\ \sum_{j=1}^n \tilde{a}_{nj}(\underline{\omega_n} - \overline{\omega_j}) \end{bmatrix},$$

where $\preceq$ and $\succeq$ denote the component-wise inequalities. This direct inspection shows that, for fixed L, we have that $\mathrm{conv}(\mathcal{X}) = \mathrm{conv}(\mathrm{vert}(\mathcal{X}))$, that is the extremal values of the solution x are achieved for extremal parameters $\omega \in \mathrm{vert}(\mathbf{\Omega})$.

Since the parametric variations $L \in \mathcal{L}$ and $\omega \in \mathbf{\Omega}$ are independent of each other, the lemma follows. ∎

We obtain the following corollary to Lemma 5.

Corollary 5. (Extremal solutions for extremal parameters) *Consider the interval-valued Laplacian equation* [**21**] *and let $c \in \mathbb{R}^n$. Then extremal values for $c^T x = c^T L^\dagger\omega$ are obtained for extremal parameters, that is,*

$$\begin{aligned} \max_{L\in\mathcal{L}\,,\,\omega\in\mathbf{\Omega}} c^T L^\dagger\omega &= \max_{L\in\mathrm{vert}(\mathcal{L})\,,\,\omega\in\mathrm{vert}(\mathbf{\Omega})} c^T L^\dagger\omega\,, \\ \min_{L\in\mathcal{L}\,,\,\omega\in\mathbf{\Omega}} c^T L^\dagger\omega &= \min_{L\in\mathrm{vert}(\mathcal{L})\,,\,\omega\in\mathrm{vert}(\mathbf{\Omega})} c^T L^\dagger\omega\,. \end{aligned}$$

Proof The proof is based on the analysis in [48, Theorem 2]. We prove only the maximizing case here. The proof for the minimizing case can be obtained analogously.

Since the sets $\mathcal{L}$ and $\mathbf{\Omega}$ are compact and $c^T L^\dagger\omega$ is a continuous function[6] of $\omega \in \mathbf{\Omega}$ and $L \in \mathcal{L}$, the function $c^T L^\dagger\omega$ attains its maximum for some $\omega^* \in \mathbf{\Omega}$ and $L^* \in \mathcal{L}$.

By Lemma 5, there exist matrices $L_1, \ldots, L_{|\mathcal{E}|} \in \mathrm{vert}(\mathcal{L})$, vectors $v_1, \ldots, v_n \in \mathrm{vert}(\mathbf{\Omega})$, and nonnegative numbers $\lambda_1, \ldots, \lambda_{|\mathcal{E}|}, \mu_1, \ldots, \mu_n$ with $\sum_{i=1}^{|\mathcal{E}|} \lambda_i = 1$ and $\sum_{j=1}^n \mu_j = 1$ such that $(L^*)^\dagger = \sum_{i=1}^{|\mathcal{E}|} \lambda_i L_i^\dagger$ and $\omega^* = \sum_{j=1}^n \mu_j v_j$. It follows that

$$\begin{aligned} c^T(L^*)^\dagger\omega^* &= c^T\Big(\sum\nolimits_{i=1}^{|\mathcal{E}|} \lambda_i L_i^\dagger\Big)\sum\nolimits_{j=1}^n \mu_j v_j \\ &= \sum\nolimits_{i=1}^{|\mathcal{E}|}\sum\nolimits_{j=1}^n \lambda_i\mu_j\Big(c^T L_i^\dagger v_j\Big) \\ &\leq \max_{i\in\{1,\ldots,|\mathcal{E}|\}\,,\,j\in\{1,\ldots,n\}} c^T L_i^\dagger v_j \end{aligned}$$

since any weighted average of numbers is bounded from above by the largest of the numbers. Thus, $\max_{L\in\mathcal{L},\omega\in\mathbf{\Omega}} c^T L^\dagger\omega$ is attained at a vertex of the parameter space. ∎

We are now ready to state the main result of this section. Namely, if we can guarantee the synchronization condition [**17**] for extremal parameters, then we can guarantee synchronization for all parametric variations and vice versa.

Theorem 6. (Robust synchronization) *Consider a connected network $\{G(\mathcal{V},\mathcal{E},\mathcal{A})\,,\,\omega\}$ with interval-valued weights $A \in \mathcal{A}$ and natural frequencies $\omega \in \mathbf{\Omega}$. Let $\mathcal{L}$ be the associated set of interval-valued Laplacian matrices, and let $\gamma \in [0, \pi/2[$. The following statements are equivalent.*

1) Parametric synchronization condition:

$$\Big\|B^T L^\dagger\omega\Big\|_\infty \leq \sin(\gamma) \quad \forall L \in \mathcal{L}\,,\ \omega \in \mathbf{\Omega}\,; \qquad [\mathbf{22}]$$

2) Worst-case synchronization condition:

$$\max_{L\in\mathrm{vert}(\mathcal{L})\,,\,\omega\in\mathrm{vert}(\mathbf{\Omega})} \Big\|B^T L^\dagger\omega\Big\|_\infty \leq \sin(\gamma)\,. \qquad [\mathbf{23}]$$

Proof The kth row of B^T reads as $b_k^T = e_i^n - e_j^n$, where $\{i,j\} \in \mathcal{E}$. Thus condition [**22**] is true if and only if

$$\begin{aligned} \sin(\gamma) \geq \max_{L\in\mathcal{L}\,,\,\omega\in\mathbf{\Omega}} \Big\|B^T L^\dagger\omega\Big\|_\infty &= \max_k \max_{L\in\mathcal{L}\,,\,\omega\in\mathbf{\Omega}} \Big|b_k^T L^\dagger\omega\Big| \\ &= \max_k \max_{L\in\mathrm{vert}(\mathcal{L})\,,\,\omega\in\mathrm{vert}(\mathbf{\Omega})} \Big|b_k^T L^\dagger\omega\Big| \\ &= \max_{L\in\mathrm{vert}(\mathcal{L})\,,\,\omega\in\mathrm{vert}(\mathbf{\Omega})} \Big\|B^T L^\dagger\omega\Big\|_\infty\,, \end{aligned}$$

where the second equality follows from Corollary 5. The latter statement is equivalent to condition [**23**]. ∎

The robust synchronization condition [**23**] in Theorem 6 is exact, but its evaluation is computationally expensive since all vertices of the parameter-space need to be sampled in a combinatorial way. We found that randomized Monte Carlo sampling methods or simplex-type algorithms perform well in practice and quickly deliver an accurate estimate of the quantity $\max_{L\in\mathrm{vert}(\mathcal{L})\,,\,\omega\in\mathrm{vert}(\mathbf{\Omega})} \big\|B^T L^\dagger\omega\big\|_\infty$. For certain topologies, such as acyclic ones, it is also possible to analytically determine the maximizing vertices beforehand, and the combinatorial condition [**23**] reduces to a scalar one. In the section *Synchronization Assessment for Power Networks*, Theorem 6 is illustrated with different examples.

Statistical Synchronization Assessment

After having established that the synchronization condition [**17**] is necessary and sufficient for particular network topologies and parameters, we now validate both its correctness and its accuracy for arbitrary networks.

[6] Continuity of $L^\dagger\omega$ with respect to the weights a_{ij} follows since $L^\dagger\omega = Q^{-1}\omega$, Q is a continuous function of a_{ij}, and the inverse of a matrix is a continuous function of its elements.

Statistical Assessment of Correctness. Extensive simulation studies lead us to the conclusion that condition **[17]** is correct in general and guarantees the existence of a stable equilibrium $\theta^* \in \bar{\Delta}_G(\gamma)$. In order to validate this hypothesis we invoke probability estimation through Monte Carlo techniques, see [50, Section 9] and [51, Section 3] for a comprehensive review.

We consider the following *nominal random networks* $\{G(\mathcal{V},\mathcal{E},A),\omega\}$ parametrized by the number $n \geq 2$ of nodes, the width $\alpha > 0$ of the sampling region for each natural frequency ω_i and $i \in \{1,\dots,n\}$, and a connected random graph model $\mathrm{RGM}(p) = G(\mathcal{V},\mathcal{E}(p))$ with node set $\mathcal{V} = \{1,\dots,n\}$ and edge set $\mathcal{E} = \mathcal{E}(p)$ induced by a coupling parameter $p \in [0,1]$. In particular, given the four parameters $(n,\mathrm{RGM},p,\alpha)$, a nominal random network is constructed as follows:

(i) Network topology: To construct the network topology, we consider three different one-parameter families of random graph models $\mathrm{RGM}(p) = G(\mathcal{V},\mathcal{E}(p))$, each parameterized by the number of nodes $n \geq 2$ and a coupling parameter $p \in [0,1]$. Specifically, we consider (i) an Erdös-Rényi random graph model (RGM = ERG) with probability p of connecting two nodes, (ii) a random geometric graph model (RGM = RGG) with sampling region $[0,1]^2 \subset \mathbb{R}^2$, connectivity radius p, and (iii) a Watts-Strogatz small world network (RGM = SMN) [52] with initial coupling of each node to its two nearest neighbors and rewiring probability p. If, for a given $n \geq 2$ and $p \in [0,1]$, the realization of a random graph model is not connected, then this realization is discarded and new realization is constructed;

(ii) Coupling weights: For a given random graph $G(\mathcal{V},\mathcal{E}(p))$, for each edge $\{i,j\} \in \mathcal{E}(p)$, the coupling weight $a_{ij} = a_{ji} > 0$ is sampled from a uniform distribution supported on the interval $[1,10]$;

(iii) Natural frequencies: For a given $n \geq 2$ and $\alpha > 0$, the natural frequencies $\omega \in \mathbf{1}_n^\perp$ are constructed in two steps. In a first step, n real numbers q_i, $i \in \{1,\dots,n\}$, are sampled from a uniform distribution supported on $[-\alpha,+\alpha]$, where $\alpha > 0$. In a second step, by subtracting the average $\sum_{i=1}^n q_i/n$ we define $\omega_i = q_i - \sum_{i=1}^n q_i/n$ for $i \in \{1,\dots,n\}$ and obtain $\omega = (\omega_1,\dots,\omega_n) \in \mathbf{1}_n^\perp$; and

(iv) Parametric realizations: We consider forty realizations of the parameter 4-tuple $(n,\mathrm{RGM},p,\alpha)$ covering a wide range of network sizes n, coupling parameters p, and natural frequencies ω, which are listed in the first column of Table 1. The choices of α in these forty cases is such that[7] the resulting equilibrium angles θ^* satisfy on average $\max_{\{i,j\}\in\mathcal{E}} |\theta_i^* - \theta_j^*| \approx \pi/3$.

For each of the forty parametric realizations in *(iv)*, we generate 30000 nominal models of $\omega \in \mathbf{1}_n^\perp$ and $G(\mathcal{V},\mathcal{E},A)$ (conditioned on connectivity) as detailed in *(i) - (iii)* above, each satisfying $\|B^T L^\dagger \omega\|_\infty < 1$. If a sample does not satisfy $\|B^T L^\dagger \omega\|_\infty < 1$, it is discarded and a new sample is generated. Hence, we obtain $1.2 \cdot 10^6$ nominal random networks $\{G(\mathcal{V},\mathcal{E},A),\omega\}$, each with a connected graph $G(\mathcal{V},\mathcal{E},A)$ and $\omega \in \mathbf{1}_n^\perp$ satisfying $\|B^T L^\dagger \omega\|_\infty \leq \sin(\gamma)$ for some $\gamma < \pi/2$.

For each case and each instance, we numerically solve equation **[7]** with accuracy 10^{-6} and test the hypothesis

$$\mathcal{H}: \left\| B^T L^\dagger \omega \right\|_\infty \leq \sin(\gamma) \implies \exists\, \theta^* \in \bar{\Delta}_G(\gamma)$$

with an accuracy 10^{-4}. The results are reported in Table 1 together with the empirical probability that the hypothesis $\mathcal{H}$ is true for a set of parameters $(n,\mathrm{RGM},p,\alpha)$. Given a set of parameters $(n,\mathrm{RGM},p,\alpha)$ and 30000 samples, the empirical probability is calculated as

$$\widehat{\texttt{Prob}}_{(n,\mathrm{RGM},p,\alpha)} = \frac{\text{number of samples satisfying } \big(\mathcal{H}\,\texttt{is true}\big)}{30000}\,.$$

Given an accuracy level $\epsilon \in]0,1[$ and a confidence level $\eta \in]0,1[$, we ask for the number of samples N such that the true probability $\texttt{Prob}_{(n,\mathrm{RGM},p,\alpha)}\big(\mathcal{H}\,\texttt{is true}\big)$ equals the empirical probability $\widehat{\texttt{Prob}}_{(n,\mathrm{RGM},p,\alpha)}$ with confidence level greater than $1-\eta$ and accuracy at least ϵ, that is,

$$\texttt{Prob}\Big(\big|\texttt{Prob}_{(n,\mathrm{RGM},p,\alpha)}\big(\mathcal{H}\,\texttt{is true}\big) - \widehat{\texttt{Prob}}_{(n,\mathrm{RGM},p,\alpha)}\big| < \epsilon\Big) > 1-\eta\,.$$

By the Chernoff-Hoeffding bound (see [50, Equation (9.14)] and [53, Theorem 1]), the number of samples N for a given accuracy ϵ and confidence η is given as

$$N \geq \frac{1}{2\epsilon^2}\log\frac{2}{\eta}. \qquad \textbf{[24]}$$

For $\epsilon = \eta = 0.01$, inequality **[24]** is satisfied for $N \geq 26492$ samples. By invoking the Chernoff-Hoeffding bound **[24]**, our simulations studies establish the following statement:

> With 99% confidence level, there is at least 99% accuracy that the hypothesis $\mathcal{H}$ is true with probability 99.97 % for a nominal network constructed as in *(i)* - *(iv)* above.
>
> In particular, for a nominal network with parameters $(n,\mathrm{RGM},p,\alpha)$ constructed as in *(i)* - *(iv)* above, with 99% confidence level, there is at least 99% accuracy that the probability $\texttt{Prob}_{(n,\mathrm{RGM},p,\alpha)}\big(\mathcal{H}\,\texttt{is true}\big)$ equals the empirical probability $\widehat{\texttt{Prob}}_{(n,\mathrm{RGM},p,\alpha)}$, as listed in Table 1, that is,
>
> $$\texttt{Prob}\Big(\big|\texttt{Prob}_{(n,\mathrm{RGM},p,\alpha)}\big(\mathcal{H}\ \texttt{is true}\big) - \widehat{\texttt{Prob}}_{(n,\mathrm{RGM},p,\alpha)}\big| < 0.01\Big) > 0.99\,.$$

It can be seen in Table 1 that for large and dense networks the hypothesis $\mathcal{H}$ is always true, whereas for small and sparsely connected networks the hypothesis $\mathcal{H}$ can marginally fail with an error of order $\mathcal{O}(10^{-4})$. Thus, for these cases a tighter condition of the form $\|B^T L^\dagger \omega\|_\infty \leq \sin(\gamma) - \mathcal{O}(10^{-4})$ is required to establish the existence of $\theta^* \in \bar{\Delta}_G(\gamma)$. These results strongly suggest that "degenerate" topologies and parameters (such as the large and isolated cycles used in the proof of Theorem 3 and in Example 1) are more likely to occur in small networks.

Statistical Assessment of Accuracy. As established in the previous subsection, the synchronization condition **[17]** is a scalar synchronization test with predictive power for almost all network topologies and parameters. This remarkable fact is difficult to establish via statistical studies in the vast parameter space. Since we proved in statement (G4) of Theorem 2 that condition **[17]** is exact for sufficiently small pairwise phase cohesiveness $|\theta_i - \theta_j| \ll 1$ (or equivalently, for sufficiently identical natural frequencies ω_i and sufficiently strong coupling), we investigate the other extreme

[7] For a fixed weighted graph $G(\mathcal{V},\mathcal{E},A)$, the feasibility of equation **[7]** and the properties of its solution θ^* are entirely determined by the remaining parameter $\alpha > 0$. If α is chosen too large, then there exists no solution θ^* of the form $\max_{\{i,j\}\in\mathcal{E}} |\theta_i^* - \theta_j^*| \leq \pi/2$. Likewise, if α is chosen too small, then $\omega \in \mathbf{1}_n^\perp$ will be nearly the zero vector, and we fall into the case (G4) of Theorem 2, that is, the angles are perfectly aligned. In order to strike a balance between these extreme cases, we choose α such that the samples yield on average $\max_{\{i,j\}\in\mathcal{E}} |\theta_i^* - \theta_j^*| \approx \pi/3$.

$\max_{\{i,j\}\in\mathcal{E}} |\theta_i-\theta_j| = \pi/2$. To test the corresponding synchronization condition **[16]** in a low-dimensional parameter space, we consider a complex network of Kuramoto oscillators

$$\dot{\theta}_i = \omega_i - K \cdot \sum_{j=1}^{n} a_{ij} \sin(\theta_i - \theta_j), \quad i \in \{1,\dots,n\}, \ \textbf{[25]}$$

where $K > 0$ is the coupling gain among the oscillators and the coupling weights are assumed to be unit-weighted, that is, $a_{ij} = a_{ji} = 1$ for all $\{i,j\} \in \mathcal{E}$. If L is the unweighted Laplacian matrix, then condition **[16]** reads as $K > K_{\text{critical}} \triangleq \|L^{\dagger}\omega\|_{\mathcal{E},\infty}$. Of course, the condition $K > K_{\text{critical}}$ is only sufficient and synchronization may occur for a smaller value of K than K_{critical}. In order to test the accuracy of the condition $K > K_{\text{critical}}$, we numerically found the smallest value of K leading to synchrony for various network sizes, connected random graph models, and sample distributions of the natural frequencies. Here we discuss in detail the construction of the random network topologies and parameters leading to the data displayed in Figure 3 of the main manuscript.

We consider the following *nominal random networks* $\{G(\mathcal{V},\mathcal{E},A),\omega\}$ parametrized by the number of nodes $n \in \{10,20,40,160\}$, the sampling distribution SD for the natural frequencies $\omega \in \mathbf{1}_n^{\perp}$, and a connected random graph model $\text{RGM}(p) = G(\mathcal{V},\mathcal{E}(p))$ with node set $\mathcal{V} = \{1,\dots,n\}$ and edge set $\mathcal{E} = \mathcal{E}(p)$ induced by a coupling parameter $p \in [0,1]$. In particular, given the four parameters $(n, \text{RGM}, p, \text{SD})$, a nominal random network is constructed as follows:

(i) Network topology and weights: To construct the network topology, we consider three different one-parameter families of random graph models $\text{RGM}(p) = G(\mathcal{V},\mathcal{E}(p))$, each parameterized by the number of nodes n and a coupling parameter $p \in [0,1]$. Specifically, we consider (i) an Erdös-Rényi random graph model (RGM = ERG) with probability p of connecting two nodes, (ii) a random geometric graph model (RGM = RGG) with sampling region $[0,1]^2 \subset \mathbb{R}^2$, connectivity radius p, and (iii) a Watts-Strogatz small world network (RGM = SMN) [52] with initial coupling of each node to its two nearest neighbors and rewiring probability p. If, for a given n and $p \in [0,1]$, the realization of a random graph model is not connected, then this realization is discarded and new realization is constructed. All nonzero coupling weights are set to one, that is, $a_{ij} = a_{ji} = 1$ for $\{i,j\} \in \mathcal{E}$;

(ii) Natural frequencies: For a given network size n and sampling distribution SD, the natural frequencies $\omega \in \mathbf{1}_n^{\perp}$ are constructed in three steps. In a first step, the sampling distribution of the natural frequencies is chosen. For classic Kuramoto oscillators with uniform coupling $a_{ij} = K/n$ for distinct $i,j \in \{1,\dots,n\}$, we know that the two extreme sampling distributions (with bounded support) are the bipolar discrete and the uniform distribution leading to the largest and smallest critical coupling, respectively [9]. Here we choose a uniform distribution (SD = uniform) supported on $[-1,+1]$ or a bipolar discrete distribution (SD = bipolar) supported on $\{-1,+1\}$. In a second step, n real numbers q_i, $i \in \{1,\dots,n\}$, are sampled from the distribution SD. In a third step, by subtracting the average $\sum_{i=1}^{n} q_i/n$ we define $\omega_i = q_i - \sum_{i=1}^{n} q_i/n$ for $i \in \{1,\dots,n\}$ and obtain $\omega = (\omega_1,\dots,\omega_n) \in \mathbf{1}_n^{\perp}$; and

(iii) Parametric realizations: We consider 600 realizations of parameter 4-tuple $(n, \text{RGM}, p, \text{SD})$ covering a wide range of network sizes n, coupling parameters p, and natural frequencies ω. All 600 realizations are shown in Figure 3 in the main manuscript.

For each of the 600 parametric realizations in *(iii)*, we generate 100 nominal models of $\omega \in \mathbf{1}_n^{\perp}$ and $G(\mathcal{V},\mathcal{E},A)$ (conditioned on connectivity) as detailed in *(i)* - *(ii)* above. Hence, we obtain 60000 nominal random networks $\{G(\mathcal{V},\mathcal{E},A),\omega\}$, each with a connected graph $G(\mathcal{V},\mathcal{E},A)$ and natural frequencies $\omega \in \mathbf{1}_n^{\perp}$. For each sample network, we consider the complex Kuramoto model **[25]** and numerically find the smallest value of K leading to synchrony with cohesive phases satisfying $\max_{\{i,j\}\in\mathcal{E}} |\theta_i - \theta_j| = \pi/2$. The critical value of K is found iteratively by integrating the Kuramoto dynamics **[25]** and decreasing K if the steady state θ^* satisfies $\max_{\{i,j\}\in\mathcal{E}} |\theta_i^* - \theta_j^*| < \pi/2$ and increasing K otherwise. We repeat this iteration until a steady state θ^* is found satisfying $\max_{\{i,j\}\in\mathcal{E}} |\theta_i - \theta_j| = \pi/2$ with accuracy 10^{-3}. Our findings are reported in Figure 3 in the main manuscript, where each data point corresponds to the sample mean of 100 nominal models with the same parameter 4-tuple $(n, \text{RGM}, p, \text{SD})$.

Synchronization Assessment for Power Networks

We envision that our proposed condition **[17]** can be applied to quickly assess synchronization and robustness in power networks under volatile operating conditions. Since real-world power networks are carefully engineered systems with particular network topologies and parameters, they cannot be reduced to the standard topological random graph models [54], and we do not extrapolate the statistical results from the previous section to power grids. Rather, we consider ten widely-established and commonly studied IEEE power network test cases provided by [55, 56] to validate the correctness and the predictive power of our synchronization condition **[17]**.

Statistical Synchronization Assessment for IEEE Systems. We validate the synchronization condition **[17]** in a smart power grid scenario subject to fluctuations in load and generation and equipped with fast-ramping generation and controllable demand. Here, we report the detailed simulation setup leading to the results shown in Table 1 of the main manuscript.

The nominal simulation parameters for the ten IEEE test cases can be found in [55, 56]. Under nominal operating conditions, the power generation is optimized to meet the forecast demand, while obeying the AC power flow laws and respecting the thermal limits of each transmission line. Thermal limits constraints are precisely equivalent to phase cohesiveness requirements, that is, for each line $\{i,j\}$, the angular distance $|\theta_i - \theta_j|$ needs to be bounded such that the corresponding power flow $a_{ij}\sin(\theta_i - \theta_j)$ is bounded. Here, we found the optimal generator power injections through the standard optimal power flow solver provided by *MATPOWER* [55].

In order to test the synchronization condition **[17]** in a volatile smart grid scenario, we make the following changes to the nominal IEEE test cases with optimal generation:

(i) *Fluctuating loads with stochastic power demand:* We assume fluctuating demand and randomize 50% of all loads (selected independently with identical distribution) to deviate from the forecasted loads with Gaussian statistics (with nominal power injection as mean and standard deviation 0.3 in per unit system);

(ii) *Renewables with stochastic power generation:* We assume that the grid is penetrated by renewables with severely fluctuating power outputs, for example, wind or solar farms, and we randomize 33% of all generating units (selected independently with identical distribution) to deviate from the nominally scheduled generation with Gaussian statistics (with nominal power injection as mean and standard deviation 0.3 in per unit system); and

(iii) *Fast-ramping generation and controllable loads:* Following the paradigm of *smart operation of smart grids* [57], the fluctuations can be mitigated by fast-ramping generation, such as fast-response energy storage including batteries and flywheels, and controllable loads, such as large-scale server farms or fleets of plug-in hybrid electrical vehicles. Here, we assume that the grid is equipped with 10% fast-ramping generation (10% of all generators, selected independently with identical distribution) and 10% controllable loads (10% of all loads, selected independently with identical distribution), and the power imbalance (caused by fluctuating demand and generation) is uniformly dispatched among these adjustable power sources.

For each of the ten IEEE test cases with optimal generator power injections, we construct 1000 random realizations of the scenario (i)-(iii) described above. For each realization, we numerically check for the existence of a solution $\theta^* \in \bar{\Delta}_G(\gamma)$, $\gamma \in [0, \pi/2[$ to the AC power flow equations, the right-hand side of the power network dynamics [4]-[5], given by

$$\begin{aligned} P_{\mathrm{m},i} &= \sum\nolimits_{j=1}^{n} a_{ij} \sin(\theta_i - \theta_j)\,, \quad i \in \mathcal{V}_1\,, \\ P_{\mathrm{l},i} &= -\sum\nolimits_{j=1}^{n} a_{ij} \sin(\theta_i - \theta_j)\,, \quad i \in \mathcal{V}_2\,. \end{aligned} \qquad [26]$$

The solution to the AC power flow equations [26] is found via the AC power flow solver provided by *MATPOWER* [55]. Notice that, by Lemma 2, if such a solution θ^* exists, then it is unique (up to rotational invariance) and also locally exponentially stable with respect to the power network dynamics [4]-[5]. Next, we compare the numerical solution θ^* with the results predicted by our synchronization condition [17]. As discussed in Remark 3, a physical insightful and computationally efficient way to evaluate condition [17] is to solve the sparse and linear DC power flow equations given by

$$\begin{aligned} P_{\mathrm{m},i} &= \sum\nolimits_{j=1}^{n} a_{ij} (\delta_i - \delta_j)\,, \quad i \in \mathcal{V}_1\,, \\ P_{\mathrm{l},i} &= -\sum\nolimits_{j=1}^{n} a_{ij} (\delta_i - \delta_j)\,, \quad i \in \mathcal{V}_2\,. \end{aligned} \qquad [27]$$

The solution δ^* of the DC power flow equations [27] is defined uniquely up to the usual translational invariance. Given the solution δ^* of the DC power flow equations [27], the left-hand side of our synchronization condition [17] evaluates to $\|B^T L^\dagger \omega\|_\infty = \|L^\dagger \omega\|_{\mathcal{E},\infty} = \max_{\{i,j\}\in\mathcal{E}} |\delta_i^* - \delta_j^*|$.

Finally, we compare our prediction with the numerical results. If $\|B^T L^\dagger \omega\|_\infty \leq \sin(\gamma)$ for some $\gamma \in [0, \pi/2[$, then condition [17] predicts that there exists a stable solution $\theta \in \bar{\Delta}_G(\gamma)$, or alternatively $\theta \in \bar{\Delta}_G(\arcsin(\|B^T L^\dagger \omega\|_\infty))$. To validate this hypothesis, we compare the numerical solution θ^* to the AC power flow equations [26] with our prediction $\theta^* \in \bar{\Delta}_G(\arcsin(\|B^T L^\dagger \omega\|_\infty))$. Our findings and the detailed statistics are reported in Table 1 of the main manuscript. It can be observed that condition [17] predicts the correct phase cohesiveness $|\theta_i^* - \theta_j^*|$ along all transmission lines $\{i,j\} \in \mathcal{E}$ with extremely high accuracy even for large-scale networks, such as the Polish power grid model featuring 2383 nodes.

Simulation Data for IEEE Reliability Test System 96. The IEEE Reliability Test System 1996 (RTS 96) is a widely adopted and relatively large-scale power network test case, which has been designed as a benchmark model for power flow and stability studies. The RTS 96 is a multi-area model featuring 40 load buses and 33 generation buses, as illustrated in Figure 4 in the main manuscript. The network parameters and the dynamic generator parameters can be found in [56].

The quantities a_{ij} in the coupled oscillator model [1] correspond to the product of the voltage magnitudes at buses i and j as well the susceptance of the transmission line connecting buses i and j. For a given set of power injections at the buses and branch parameters, the voltage magnitudes and initial phase angles were calculated using the optimal power flow solver provided by *MATPOWER* [55]. The quantities ω_i, $i \in \mathcal{V}_2$, are the real power demands at loads, and ω_i, $i \in \mathcal{V}_1$, are the real power injections at the generators, which were found through the optimal power flow solver provided by *MATPOWER* [55]. We made the following changes in order to adapt the detailed RTS 96 model to the classic structure-preserving power network model [4]-[5] describing the generator rotor and voltage phase dynamics. First, we replaced the synchronous condenser in the original RTS 96 model [56] by a U50 hydro generator. Second, since the numerical values of the damping coefficients D_i are not contained in the original RTS 96 description [56], we chose the following values to be found in [16]: for the generator damping, we chose the uniform damping coefficient $D_i = 1$ in per unit system and for $i \in \mathcal{V}_1$, and for the load frequency coefficient we chose $D_i = 0.1\,\mathrm{s}$ for $i \in \mathcal{V}_2$. Third and finally, we discarded an optional high voltage DC link for the branch $\{113, 316\}$.

Bifurcation Scenario in the IEEE Reliability Test System 96. As shown in the main manuscript, an imbalanced power dispatch in the RTS 96 network together with a tripped generator (generator 323) in the Southeastern (green) area results in a loss of synchrony since the maximal power transfer is limited due to thermal constraints. This loss of synchrony can be predicted by our synchronization condition [17] with extremely high accuracy. In the following, we show that a similar loss of synchrony occurs, even if the generator 323 is not disconnected and there are no thermal limit constraints on the transmission lines. In this case, the loss of synchrony is due to a saddle node bifurcation at an inter-area angle of $\pi/2$, which can be predicted accurately by condition [17] as well.

For the following dynamic simulation we consider again an imbalanced power dispatch: the demand at each load in the Southeast (green) area is increased by a uniform amount and the resulting power imbalance is compensated by uniformly increasing the generation at each generator in the two Western (blue) areas. The imbalanced power dispatch essentially transforms the RTS 96 into a two-oscillator network, and we observe the classic loss of synchrony through a saddle-node bifurcation [9, 18] shown in Figures 11 and 12. In particular, the network is still synchronized for a load increase of 141% resulting in $\left\|L^\dagger \omega\right\|_{\mathcal{E},\infty} = 0.9995 < 1$. If the loads are increased by an additional 10% resulting in $\left\|L^\dagger \omega\right\|_{\mathcal{E},\infty} = 1.0560 > 1$, then synchronization is lost and the areas separate via the transmission lines $\{121, 325\}$ and $\{223, 318\}$. In summary, this transmission line scenario nicely illustrates the correctness and the accuracy of the proposed condition [16].

We want to state two remarks on this bifurcation scenario and its extensions to more detailed power network models. As discussed in Remark 1, the underlying modeling assumption of constant voltage magnitudes at the loads may not be true near the bifurcation point, and a higher-order model including voltage dynamics and reactive power flow equations may reveal different dynamics than the considered model [4]-[5]. Additionally, in real-world power networks the transmission lines $\{121, 325\}$ and $\{223, 318\}$ would be separated at some smaller inter-area angle $\gamma^* \ll \pi/2$ due to thermal limit constraints on the transmission lines. This separation at the angle γ^* can also be predicted accurately from condition [17], see the analysis and results in the main paper.

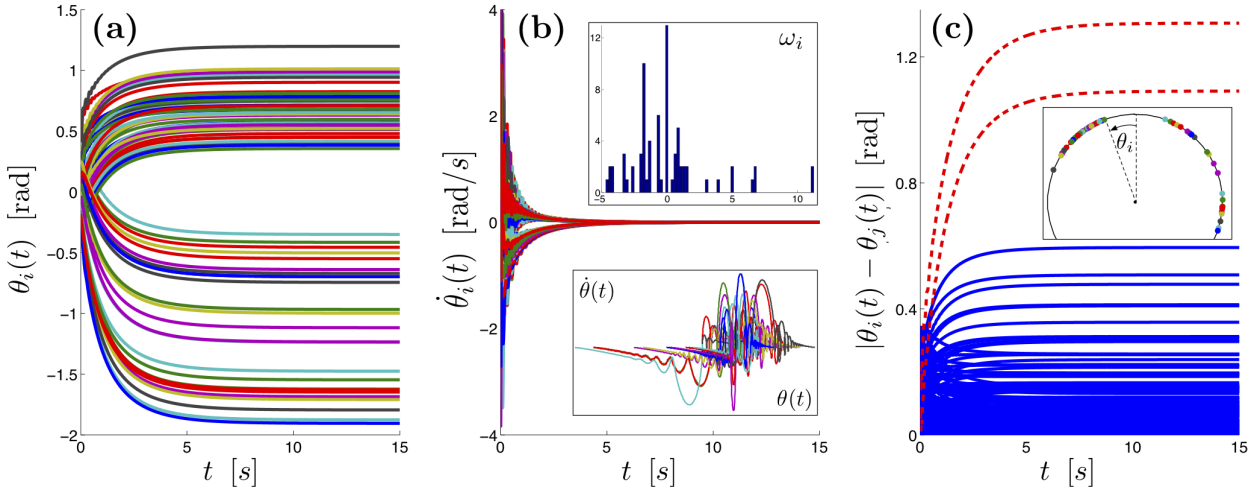

Fig. 11. Time series of the RTS 96 dynamics for 141% load increase resulting in $\|B^T L^\dagger \omega\|_\infty = \|L^\dagger \omega\|_{\mathcal{E},\infty} = 0.9995 < 1$. Figure **(a)** depicts the angles $\theta_i(t)$, Figure **(b)** shows the frequencies $\dot{\theta}_i(t)$, and Figure **(c)** depicts the angular distances $|\theta_i(t) - \theta_j(t)|$ over transmission lines, where the red dashed curves correspond to the pairs $\{121, 325\}$ and $\{223, 318\}$. The inserts show the power injections ω_i, the phase space of the generator dynamics $(\theta(t), \dot{\theta}(t))$, and the stationary angles θ_i.

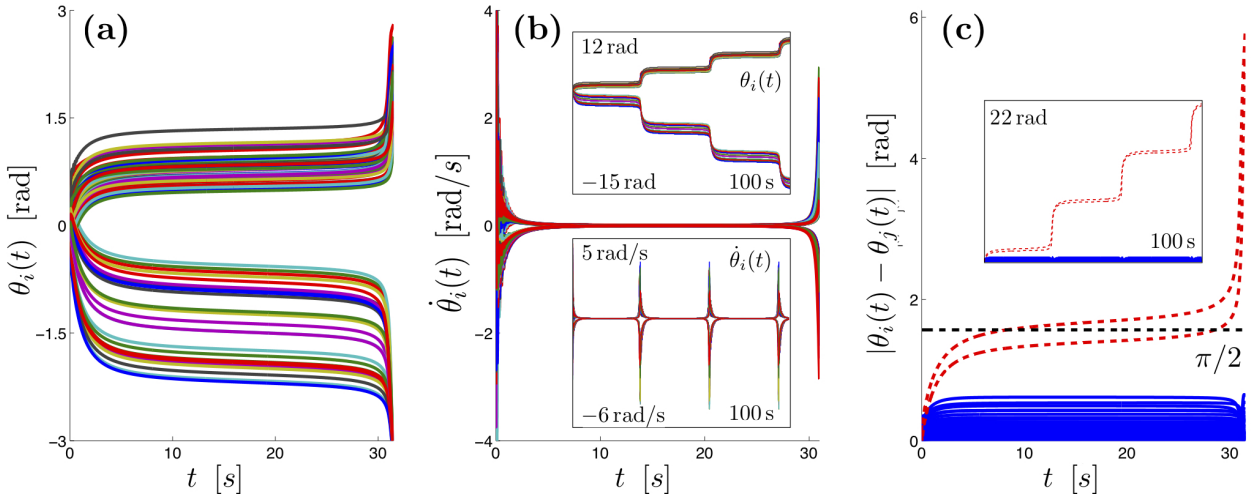

Fig. 12. Time series of the RTS 96 dynamics for 151% load increase resulting in $B^T L^\dagger \omega\|_\infty = \|L^\dagger \omega\|_{\mathcal{E},\infty} = 1.0560 > 1$. Figure **(a)** depicts the angles $\theta_i(t)$, Figure **(b)** depicts the frequencies $\dot{\theta}_i(t)$, and Figure **(c)** depicts the angular distances $|\theta_i(t) - \theta_j(t)|$ over transmission lines, which diverge for the pairs $\{121, 325\}$ and $\{223, 318\}$ shown as red dashed curves. The inserts depict the long-time dynamics simulated over 100s.

Synchronization Assessment in Presence of Non-Constant Voltages and Power Demands. As discussed in Remark 1, the underlying modeling assumption of constant voltage magnitudes at the loads is idealistic and not always true. For example, if the loads demand a constant amount of active and reactive power (rather than demanding constant power and voltage), then the load bus voltages have to follow the power demand, and the coupling weights $a_{ij} = |V_i| \cdot |V_j| \cdot \Im(Y_{ij})$ cannot be regarded as a-priori known and constant parameters. Likewise, the active power demand ω_i at the loads is variable and can only be predicted with a certain accuracy.

In the following, we overapproximate uncertain parameters and unmodeled dynamics by the interval-valued parameters $\underline{\omega_i} \leq \omega_i \leq \overline{\omega_i}$ and $0 < \underline{a_{ij}} \leq a_{ij} \leq \overline{a_{ij}}$ and apply the analysis developed in the section *Robust Synchronization in Presence of Uncertainty*. To verify the accuracy of the proposed robust synchronization condition **[23]**, we repeat similar numerical experiments as in the subsection *Statistical Synchronization Assessment for IEEE Systems*. We consider four representative IEEE test cases of different sizes (9 bus system by Chow, IEEE 14, IEEE 39 New England, and IEEE 118) with optimal generator power injections, and we make the following changes to theses nominal test cases:

(i) *Fluctuating loads with stochastic active and reactive power demand:* We assume fluctuating demand and randomize *all* loads to deviate from their nominal values with Gaussian statistics, with nominal active and reactive power demands as mean, a standard deviation 0.3 (in per unit system) for the reactive power demand, and standard deviation 0.05 (in per unit system) for the active power demand.

(ii) *Fast-ramping generation:* We assume that the grid is equipped with 20% fast-ramping generation (20% of all generators, selected independently with identical distribution), and the active power imbalance (caused by fluctuating demand) is uniformly dispatched among these adjustable power sources. Notice that the fast-ramping generators do not provide any reactive power support for the

fluctuating reactive power demands at the loads, which results in highly variable load bus voltages.

For each of the ten IEEE test cases, we construct 1000 random realizations of the scenario (i)-(ii) described above. For each realization, we numerically check for the existence of a solution $\theta^* \in \bar{\Delta}_G(\gamma)$, $\gamma \in [0, \pi/2[$ to the active power flow equations **[26]**. Here, the parameters $a_{ij} = |V_i| \cdot |V_j| \cdot \Im(Y_{ij})$ are found by solving the reactive power balance equations using *MATPOWER* [55]. After obtaining all network samples and their solutions, we construct the left-hand side of our robust synchronization condition **[23]**, $\max_{L \in \mathrm{vert}(\mathcal{L}),\, \omega \in \mathrm{vert}(\mathbf{\Omega})} \left\| B^T L^\dagger \omega \right\|_\infty$. Next, we compare the numerical solution θ^* (obtained for each sample) with the robust synchronization condition **[23]**, which predicts that $\theta^* \in \bar{\Delta}_G(\arcsin(\max_{L \in \mathrm{vert}(\mathcal{L}),\, \omega \in \mathrm{vert}(\mathbf{\Omega})} \left\| B^T L^\dagger \omega \right\|_\infty))$. Our findings are reported are reported in Table 2.

First observe from Table 2 that the load voltages and power injections fluctuate severely, and the resulting interval-valued parameters $\underline{\omega_i} \leq \omega_i \leq \overline{\omega_i}$ and $0 < \underline{a_{ij}} \leq a_{ij} \leq \overline{a_{ij}}$ are allowed to vary in relatively large domains. Despite these severe uncertainties, it can be observed that the robust synchronization condition **[23]** still predicts the correct phase cohesiveness $|\theta_i^* - \theta_j^*|$ along all transmission lines $\{i,j\} \in \mathcal{E}$ with relatively high accuracy. Of course, the results in Table 2 are more conservative than those in Table 1 of the main manuscript since condition **[23]** is based on an overapproximation of the detailed power network dynamics, that is, certain vertices of the set $\{\mathrm{vert}(\mathcal{L}), \mathrm{vert}(\mathbf{\Omega})\}$ do not occur when numerically solving a detailed power network model, and they are the dominant source for the accuracy errors in Table 2.

These results show that the robust synchronization condition **[23]** is indeed capable of predicting the solutions to the active power flow equations **[26]** in presence of uncertain voltages (resulting from the unmodeled reactive power flow equations) and fluctuating loads. Conversely, if the voltage magnitudes $|V_i|$ are known to vary within reasonable prespecified bounds (for example, $|V_i| \in [0.95, 1.05]$) and the loads are predicted with high accuracy, then condition **[23]** delivers accurate results in presence of uncertainties.

Table 2. Evaluation of the worst-case condition [23] for four IEEE test cases with fluctuating demand.

Randomized test case (1000 instances):	*Correctness:	†Accuracy: [rad]	‡Cohesive phases: [rad]	§Variations in power demand [per unit]	¶Variations in voltages [per unit]
Chow 9 bus system	`always true`	0.14229	0.15637	0.79891	0.19262
IEEE 14 bus system	`always true`	0.20416	0.18429	1.0537	0.57177
New England 39	`always true`	0.048628	0.1756	0.81972	0.077967
IEEE 118 bus system	`always true`	0.097533	0.23370	0.37332	0.32301

*Correctness: $\max_{L \in \mathrm{vert}(\mathcal{L}),\, \omega \in \mathrm{vert}(\mathbf{\Omega})} \left\| B^T L^\dagger \omega \right\|_\infty \leq \sin(\gamma) \implies \max_{\{i,j\} \in \mathcal{E}} |\theta_i^* - \theta_j^*| \leq \gamma$

†Accuracy: $\max_{1000 \text{ iterations}} \left| \max_{\{i,j\} \in \mathcal{E}} |\theta_i^* - \theta_j^*| - \arcsin(\max_{L \in \mathrm{vert}(\mathcal{L}),\, \omega \in \mathrm{vert}(\mathbf{\Omega})} \left\| B^T L^\dagger \omega \right\|_\infty) \right|$

‡Phase cohesiveness: $\max_{1000 \text{ iterations}} \{ \max_{\{i,j\} \in \mathcal{E}} |\theta_i^* - \theta_j^*| \}$

§Variations in power demand: $\max_{i \in \mathcal{V}} \{ \max_{1000 \text{ iterations}} P_{l,i} - \min_{1000 \text{ iterations}} P_{l,i} \}$

¶Variations in load voltages: $\max_{i \in \mathcal{V}_2} \{ \max_{1000 \text{ iterations}} |V_i| - \min_{1000 \text{ iterations}} |V_i| \}$

1. Biggs, N. Algebraic Graph Theory (Cambridge University Press, 1994), 2 edn.
2. Biggs, N. Algebraic potential theory on graphs. Bulletin of the London Mathematical Society 29, 641–683 (1997).
3. Dörfler, F. & Bullo, F. Kron reduction of graphs with applications to electrical networks. IEEE Transactions on Circuits and Systems (2011). To appear.
4. Kuramoto, Y. Self-entrainment of a population of coupled non-linear oscillators. In Araki, H. (ed.) Int. Symposium on Mathematical Problems in Theoretical Physics, vol. 39 of Lecture Notes in Physics, 420–422 (Springer, 1975).
5. Kuramoto, Y. Chemical Oscillations, Waves, and Turbulence (Springer, 1984).
6. Strogatz, S. H. From Kuramoto to Crawford: Exploring the onset of synchronization in populations of coupled oscillators. Physica D: Nonlinear Phenomena 143, 1–20 (2000).
7. Acebrón, J. A., Bonilla, L. L., Vicente, C. J. P., Ritort, F. & Spigler, R. The Kuramoto model: A simple paradigm for synchronization phenomena. Reviews of Modern Physics 77, 137–185 (2005).
8. Winfree, A. T. The Geometry of Biological Time (Springer, 2001), 2 edn.
9. Dörfler, F. & Bullo, F. On the critical coupling for Kuramoto oscillators. SIAM Journal on Applied Dynamical Systems 10, 1070–1099 (2011).
10. Dörfler, F. & Bullo, F. Exploring synchronization in complex oscillator networks. In IEEE Conf. on Decision and Control (Maui, HI, USA, 2012). To appear.
11. Sauer, P. W. & Pai, M. A. Power System Dynamics and Stability (Prentice Hall, 1998).
12. Bergen, A. R. & Hill, D. J. A structure preserving model for power system stability analysis. IEEE Transactions on Power Apparatus and Systems 100, 25–35 (1981).
13. Sastry, S. & Varaiya, P. Hierarchical stability and alert state steering control of interconnected power systems. IEEE Transactions on Circuits and Systems 27, 1102–1112 (1980).
14. Chiang, H.-D., Chu, C. C. & Cauley, G. Direct stability analysis of electric power systems using energy functions: Theory, applications, and perspective. Proceedings of the IEEE 83, 1497–1529 (1995).
15. Dörfler, F. & Bullo, F. Synchronization and transient stability in power networks and non-uniform Kuramoto oscillators. SIAM Journal on Control and Optimization 50, 1616–1642 (2012).
16. Kundur, P. Power System Stability and Control (McGraw-Hill, 1994).
17. Simpson-Porco, J. W., Dörfler, F. & Bullo, F. Synchronization and Power Sharing for Droop-Controlled Inverters in Islanded Microgrids. Automatica (2012). Submitted.
18. Dobson, I. Observations on the geometry of saddle node bifurcation and voltage collapse in electrical power systems. IEEE Transactions on Circuits and Systems I: Fundamental Theory and Applications 39, 240–243 (1992).
19. Wu, F. F. & Kumagai, S. Limits on Power Injections for Power Flow Equations to Have Secure Solutions (Electronics Research Laboratory, College of Engineering, University of California, 1980).

20. Jadbabaie, A., Motee, N. & Barahona, M. On the stability of the Kuramoto model of coupled nonlinear oscillators. In American Control Conference, 4296–4301 (Boston, MA, USA, 2004).
21. Nishikawa, T., Motter, A. E., Lai, Y. C. & Hoppensteadt, F. C. Heterogeneity in oscillator networks: Are smaller worlds easier to synchronize? Physical Review Letters 91, 14101 (2003).
22. Arenas, A., Díaz-Guilera, A., Kurths, J., Moreno, Y. & Zhou, C. Synchronization in complex networks. Physics Reports 469, 93–153 (2008).
23. Boccaletti, S., Latora, V., Moreno, Y., Chavez, M. & Hwang, D. U. Complex networks: Structure and dynamics. Physics Reports 424, 175–308 (2006).
24. Wu, F. & Kumagai, S. Steady-state security regions of power systems. IEEE Transactions on Circuits and Systems 29, 703–711 (1982).
25. Korniss, G. et al. Scaling in small-world resistor networks. Physics Letters A 350, 324–330 (2006).
26. Buzna, L., Lozano, S. & Diaz-Guilera, A. Synchronization in symmetric bipolar population networks. Physical Review E 80, 66120 (2009).
27. Pecora, L. M. & Carroll, T. L. Master stability functions for synchronized coupled systems. Physical Review Letters 80, 2109–2112 (1998).
28. Verwoerd, M. & Mason, O. Global phase-locking in finite populations of phase-coupled oscillators. SIAM Journal on Applied Dynamical Systems 7, 134–160 (2008).
29. Strogatz, S. H. & Mirollo, R. E. Phase-locking and critical phenomena in lattices of coupled nonlinear oscillators with random intrinsic frequencies. Physica D: Nonlinear Phenomena 31, 143–168 (1988).
30. Kopell, N. & Ermentrout, G. B. Coupled oscillators and the design of central pattern generators. Mathematical Biosciences 90, 87–109 (1988).
31. Verwoerd, M. & Mason, O. On computing the critical coupling coefficient for the Kuramoto model on a complete bipartite graph. SIAM Journal on Applied Dynamical Systems 8, 417–453 (2009).
32. Gómez-Gardenes, J., Moreno, Y. & Arenas, A. Paths to synchronization on complex networks. Physical Review Letters 98, 34101 (2007).
33. Moreno, Y. & Pacheco, A. F. Synchronization of Kuramoto oscillators in scale-free networks. Europhysics Letters 68, 603 (2004).
34. Kalloniatis, A. C. From incoherence to synchronicity in the network Kuramoto model. Physical Review E 82, 066202 (2010).
35. Strogatz, S. H. Exploring complex networks. Nature 410, 268–276 (2001).
36. Tavora, C. J. & Smith, O. J. M. Stability analysis of power systems. IEEE Transactions on Power Apparatus and Systems 91, 1138–1144 (1972).
37. Tavora, C. J. & Smith, O. J. M. Equilibrium analysis of power systems. IEEE Transactions on Power Apparatus and Systems 91, 1131–1137 (1972).
38. Ilić, M. Network theoretic conditions for existence and uniqueness of steady state solutions to electric power circuits. In IEEE International Symposium on Circuits and Systems, 2821–2828 (San Diego, CA, USA, 1992).
39. Arapostathis, A., Sastry, S. & Varaiya, P. Analysis of power-flow equation. International Journal of Electrical Power & Energy Systems 3, 115–126 (1981).
40. Grijalva, S. & Sauer, P. W. A necessary condition for power flow Jacobian singularity based on branch complex flows. IEEE Transactions on Circuits and Systems I: Fundamental Theory and Applications 52, 1406–1413 (2005).
41. Sauer, P. W., Lesieutre, B. C. & Pai, M. A. Maximum loadability and voltage stability in power systems. International Journal of Electrical Power & Energy Systems 15, 145–153 (1993).
42. Chandrashekhar, K. S. & Hill, D. J. Cutset stability criterion for power systems using a structure-preserving model. International Journal of Electrical Power & Energy Systems 8, 146–157 (1986).
43. Gravagne, I. A. & Walker, I. D. On the structure of minimum effort solutions with application to kinematic redundancy resolution. IEEE Transactions on Robotics and Automation 16, 855–863 (2000).
44. Ha, I. & Lee, J. Analysis on a minimum infinity-norm solution for kinematically redundant manipulators. ICASE Transaction on Control, Automation and Systems Engineering 4, 130–139 (2002).
45. Woods, A. J. & Wollenberg, B. F. Power Generation, Operation, and Control (Wiley, 1996), 2 edn.
46. Bürger, M., Zelazo, D. & Allgöwer, F. Hierarchical clustering of dynamical networks using a saddle-point analysis. IEEE Transactions on Automatic Control (2012). To appear.
47. Ning, S. & Kearfott, R. B. A comparison of some methods for solving linear interval equations. SIAM Journal on Numerical Analysis 34, 1289–1305 (1997).
48. Brayton, R., Hoffman, A. & Scott, T. A theorem on inverses of convex sets of real matrices with application to the worst case DC problem. IEEE Transactions on Circuits and Systems 24, 409–415 (1977).
49. Dreyer, A. Interval analysis of linear analog circuits. In GAMM-IMACS International Symposium on Scientific Computing, Computer Arithmetic and Validated Numerics, 14–14 (2006).
50. Tempo, R., Calafiore, G. & Dabbene, F. Randomized Algorithms for Analysis and Control of Uncertain Systems (Springer, 2005).
51. Calafiore, G. C., Dabbene, F. & Tempo, R. Research on probabilistic methods for control system design. Automatica 47, 1279–1293 (2011).
52. Watts, D. J. & Strogatz, S. H. Collective dynamics of 'small-world' networks. Nature 393, 440–442 (1998).
53. Hoeffding, W. Probability inequalities for sums of bounded random variables. Journal of the American Statistical Association 58, 13–30 (1963).
54. Wang, Z., Scaglione, A. & Thomas, R. J. Generating statistically correct random topologies for testing smart grid communication and control networks. IEEE Transactions on Smart Grid 1, 28–39 (2010).
55. Zimmerman, R. D., Murillo-Sánchez, C. E. & Gan, D. MATPOWER: Steady-state operations, planning, and analysis tools for power systems research and education. IEEE Transactions on Power Systems 26, 12–19 (2011).
56. Grigg, C. et al. The IEEE Reliability Test System - 1996. A report prepared by the Reliability Test System Task Force of the Application of Probability Methods Subcommittee. IEEE Transactions on Power Systems 14, 1010–1020 (1999).
57. Varaiya, P. P., Wu, F. F. & Bialek, J. W. Smart operation of smart grid: Risk-limiting dispatch. Proceedings of the IEEE 99, 40–57 (2011).

Table 1. Results of the Monte Carlo simulations to test the hypothesis $\mathcal{H}$.

nominal random network parametrized by $(n, \mathrm{RGM}, p, \alpha)$	failures of hypothesis $\mathcal{H}$: # ($\mathcal{H}$ `is not true`)	empirical probability: $\widehat{\texttt{Prob}}_{(n,\mathrm{RGM},p,\alpha)}$
$(10, \mathrm{ERG}, 0.15, 6)$	104	99.653 %
$(10, \mathrm{ERG}, 0.3, 8)$	65	99.783 %
$(10, \mathrm{ERG}, 0.5, 14)$	15	99.950 %
$(10, \mathrm{ERG}, 0.75, 25)$	0	100 %
$(20, \mathrm{ERG}, 0.15, 10)$	80	99.733 %
$(20, \mathrm{ERG}, 0.3, 15)$	5	99.983 %
$(20, \mathrm{ERG}, 0.5, 24)$	0	100 %
$(20, \mathrm{ERG}, 0.75, 45)$	0	100 %
$(30, \mathrm{ERG}, 0.15, 13)$	22	99.927 %
$(30, \mathrm{ERG}, 0.3, 20)$	0	100 %
$(30, \mathrm{ERG}, 0.5, 37)$	0	100 %
$(30, \mathrm{ERG}, 0.75, 65)$	0	100 %
$(60, \mathrm{ERG}, 0.15, 20)$	1	99.997 %
$(60, \mathrm{ERG}, 0.3, 40)$	0	100 %
$(60, \mathrm{ERG}, 0.5, 70)$	0	100 %
$(60, \mathrm{ERG}, 0.75, 125)$	0	100 %
$(120, \mathrm{ERG}, 0.15, 35)$	0	100 %
$(120, \mathrm{ERG}, 0.3, 75)$	0	100 %
$(120, \mathrm{ERG}, 0.5, 130)$	0	100 %
$(120, \mathrm{ERG}, 0.75, 235)$	0	100 %
$(10, \mathrm{RGG}, 0.3, 10)$	15	99.950 %
$(10, \mathrm{RGG}, 0.5, 15)$	18	99.940 %
$(20, \mathrm{RGG}, 0.3, 10)$	23	99.924 %
$(20, \mathrm{RGG}, 0.5, 15)$	3	99.990 %
$(30, \mathrm{RGG}, 0.3, 10)$	31	99.897 %
$(30, \mathrm{RGG}, 0.5, 15)$	1	99.997 %
$(60, \mathrm{RGG}, 0.3, 10)$	3	99.990 %
$(60, \mathrm{RGG}, 0.5, 15)$	0	100 %
$(120, \mathrm{RGG}, 0.3, 10)$	0	100 %
$(120, \mathrm{RGG}, 0.5, 15)$	0	100 %
$(10, \mathrm{SMN}, 0.1, 10)$	2	99.994 %
$(10, \mathrm{SMN}, 0.2, 10)$	0	100 %
$(20, \mathrm{SMN}, 0.1, 13)$	0	100 %
$(20, \mathrm{SMN}, 0.2, 13)$	0	100 %
$(30, \mathrm{SMN}, 0.1, 10)$	0	100 %
$(30, \mathrm{SMN}, 0.2, 13)$	0	100 %
$(60, \mathrm{SMN}, 0.1, 7)$	0	100 %
$(60, \mathrm{SMN}, 0.2, 7)$	0	100 %
$(120, \mathrm{SMN}, 0.1, 4)$	0	100 %
$(120, \mathrm{SMN}, 0.2, 4)$	0	100 %
over all $1.2 \cdot 10^6$ instances	388	99.968 %

[†]Overall, $1.2 \cdot 10^6$ instances of $\{G(\mathcal{V}, \mathcal{E}, A), \omega\}$ were constructed as described in *(i)* - *(iv)* above, each satisfying $\|B^T L^\dagger \omega\|_\infty < 1$. For each instance, the fixed-point equation **[7]** was solved with accuracy 10^{-6}, and failures of the hypothesis $\mathcal{H}$ were reported within an accuracy of 10^{-4}, that is, failures of order 10^{-5} were discarded.